Thermal Investigation of a Solar Box-type Cooker with Nanocomposite Phase Change Materials Using Flexible Thermography

G. Palanikumar[a], S. Shanmugan[b], V. Chithambaram[c], Shiva Gorjian[d], Catalin I. Pruncu[e,f], F.A. Essa[g], A.E.Kabeel[h,i], Hitesh Panchal[j], B. Janarthanan[k], Hossein Ebadi[l], Ammar H. Elsheikh[m], P. Selvarajun[o]

[a]Research scholar, Research Centre of Physics, Dhanalakshmi College of Engineering, Tambaram, Chennai, Tamil Nadu, 601 301, India

[b]Research Centre for Solar Energy, Department of Physics, Koneru Lakshmaiah Education Foundation, Green Fields, Guntur District, Vaddeswaram, Andhra Pradesh, 522502, India

[c]Department of Physics, PERI Institute of Technology, Tambaram, Mannivakkam, Tamil Nadu, 600048, India

[d]Biosystems Engineering Department, Faculty of Agriculture, Tarbiat Modares University (TMU), Tehran, Iran

[e]Mechanical Engineering, Imperial College London, Exhibition Rd., London, SW7 2AZ, UK

[f]Design, Manufacturing & Engineering Management, University of Strathclyde, Glasgow, G1 1XJ, UK

[g]Mechanical Engineering Department, Faculty of Engineering, Kafrelsheikh University, Kafrelsheikh, Egypt

[h]Mechanical Power engineering department, Faculty of engineering, Tanta university, Egypt

[i]Faculty of Engineering Delta University for Science and technology Gamasa, Egypt

[j]Mechanical Engineering Department, Government Engineering College Patan, Gujarat, 384265, India

[k]Department of Physics, Karpagam Academy of Higher Education, Eachanari, Coimbatore, Tamil Nadu, 641021, India

[l]MAHTEP Group, Dipartimento Energia “Galileo Ferraris” (DENERG), Politecnico di Torino, 10129, Turin, Italy

[m]Mechanical Power Engineering Department Faculty of Engineering Tanta university Egypt, 31527, Egypt

[n]Research Centre of Energy & Mathematics, Forty-Five, Enterprises, Chennai, 600094, Tamilnadu, India

[o]Rajalakshmi Institute of Technology, Chembarambakkam, Chennai, Tamil Nadu, 600124, India

Abstract

In this study, three SBCs are developed as (i) SBC with phase change material (PCM: waste cooking oil and $C_4H_4O_3$), (ii) a novel SBC with nanocomposite PCM (NPCM), and (iii) a SBC without NPCM. The novel proposed cooker integrated with NPCM ($MgAl_2O_4$/Ni/Fe_2O_3-PCM) was experimentally developed and its performance was evaluated using fuzzy logic and Cramer’s rules, and image processing techniques. The results indicated that the implementation of a bar plate absorber coated with $MgAl_2O_4$/Ni-doped, Fe_2O_3 nanoparticles, and integrated with PCM increases the cooker's internal temperature up to 164.12°C. The used nanocomposite materials were in the average particle size of 20 μm. The cooking materials were verified with the temperature in the segmentation process. The NPCM indicated the SBC's thermal performance enhancement of 11% in comparison with the SBC with PCM and without NPCM. Additionally, the overall thermal performance of SBCs without NPCM, with PCM, and with NPCM was obtained as 24.90-33.90%, 24.77-45.20%, and 31.77-56.21%, respectively. Moreover, the temperature of the bar plate absorber was achieved as 163.74°C, 147°C, and 113.34°C for the SBC with NPCM, PCM, and without NPCM, respectively, under the solar radiation of 1,037 W/m^2.

Keywords: Nanocomposite PCM, Box-type cooker, Thermography, Thermal performance.

1 Introduction

Cooking is extremely important for human life but it depends on fossil fuels in a way that most cookers are powered by burning conventional solid fuels like coal, wood, kerosene, etc., which are polluting and bring several health risks for the users [1–3]. Hence, clean cooking must be expanded drastically and promoted particularly to the isolated regions to hamper further premature deaths. Although many developments have been made, there is still a significant demand for clean cooking so that in 2020, the number of people that suffered from the lack of cooking facilities with no pollutants was 71% of the total population in Africa, 44% in Asia, 11% in Central and South America [4,5]. Additionally, in most of the regions around the world with low access to conventional fuels as the primary energy source, the potential of solar energy is relatively high, highlighting the importance of using solar energy as an alternative energy source [6–8]. In this regard, solar-powered cooking, as one of the low-tech applications of solar energy can be employed as a sustainable cooking facility to provide food for needy communities. In a typical solar cooker, heat is trapped inside an enclosure where the internal air temperature may reach nearly 200 ºC [9] that would be sufficient to cook or bake foodstuffs.

In essence, solar cookers can be either a direct type in which sunlight reaches the cooking pot to transfer thermal energy directly or indirectly. Thermal power is provided using a solar collector and supplied to the cooking unit indirectly [10]. Direct types can be classified into solar panel cookers [11], box-type cookers [9], and concentrating cookers [12].

Numerous attempts have been made to study and develop different solar cookers to improve efficiency and broaden their applicability. Schwarzer et al. [13] showed the fundamental characteristics, design principles, and testing standards for a simple solar cooker. They reported that several criteria concerning safety, portability, stability, endurance, robustness, and user-friendliness are essential to consider for this technology. In another study, Lokeswaran and Eswaramoorthy [14] presented a solar cooker coupled with a parabolic dish concentrator (PDC) and a porous medium using scrap material. Conducting several tests indicated that implementing a porous medium increases the operating temperature, water temperature, and optical efficiency compared to the cooker with the plain receiver. Moreover, Chen et al. [15] employed a radio telescope sub-reflector to form a concentrating solar cooker and investigate the system's performance. Using both simulated and test results revealed that the solar cooker operating in tracking mode could result in an output temperature of 92.2 ºC. González-Aviles et al. [16] modified an early model of solar cookers, including a basket as a solar collector to hold the cooking pot. The results indicated that the proposed system can provide 75 W of the required power for cooking with a thermal efficiency of 20%. Another design was introduced by Edmonds [17] in which eight reflector panels concentrated the sunlight through the cooking pan with reduced optical and thermal losses. Experimental data demonstrated that the cooking temperature could reach 260 ºC under fair-weather conditions. Using a curved Fresnel lens concentrator, Zhao et al. [18] developed a solar cooker that yielded high concentration while tracked the sun. Results showed that the system could achieve 361 ºC when the beam radiation reaches 712 W/m^2, and the cooking takes 34 min when 0.5 kg of pork is cooked. Further modifications in the solar cooker as a combination with a dryer [19], integration with a parabolic trough [20], utilization of Fresnel lens with a cavity receiver [10], and incorporation with an evacuated tube [21] have also documented in the literature.

In the solar box-type cooker (SBC) as the most studied design, researchers have presented significant developments. Mahavar et al. [22] studied an SBC to find the optimum load values where the desired range was found to be 1.2 to 1.6 kg of food material. In another attempt, Farooqui [23] proposed a powerless tracking mechanism to be incorporated with the SBCs. The tracking system operated within 6 h using no external power while being powered by potential energy stored in a water container assisted with springs. A novel hybrid solar cooker consisting of photovoltaic (PV) panels to provide extra heat via direct current (DC) heaters was developed and compared to a simple solar cooker by Joshi and Jani [24]. The results revealed that the efficiency of the modified box-type cooker can be enhanced to reach 38%, while the cooking time is reduced compared with conventional methods. Harmim et al. [25] evaluated the influence of a finned absorber on the efficiency of a box-type cooker, where results demonstrated that the proposed modification increases the stagnation temperature by 7% and decreases the time required to boil the water by 12%. The integration of an electric backup unit with a SBC was also studied by Mahavar et al. [26] to facilitate the deployment of this technology despite its dependency on weather conditions. Test data suggested that this hybrid system can cook 1.2 kg of food material for 100 min on a cloudy day. The electric backup contribution was only 0.12 kWh and 82% lower than the conventional electric heater.

The implementation of reflector panels has also been reported as one of the promising techniques used in SBCs to enhance their performance. In this case, Harmim et al. [27] developed a building-integrated solar cooker using compound parabolic (CPC) reflectors, where 78.9 W of the cooking power was obtained, reaching a maximum temperature of 166°C. Furthermore, Guidara et al. [28] used four outer reflectors to improve a SBC's performance and reported that cooking times for rice and beans are 72 and 107 min, respectively. Weldu et al. [29] reported that tracking reflectors can increase the cooker thermal efficiency by 9.6% compared to fixed reflecting mirrors. The utilization of an aluminum receiver instead of stainless steel would improve thermal efficiency by 15.4%. Additional enhancement techniques have been introduced by scientists to improve the performance of SBCs which can be found in Refs. [30,31].

One of the major drawbacks of SBCs is the short length of the time for an effective operation since the desired efficiency is obtained only in specific periods in the day. The researchers have also suggested a variety of thermal storage units to improve the thermal efficiency of solar cookers. They have used different mediums including salt (53 wt% KNO_3, 40 wt% $NaNO_2$, 7 wt% $NaNO_3$) [32], Bayburt stone [33], pentaerythritol [34], galactitol [35], technical grade paraffin and erythritol [36], magnesium chloride hexahydrate [37], acetamide and stearic acid [38]. Bhave and Kale [39] showed that the use of phase change material (PCM) allows a modified solar cooker. It took about 110 min for the cooker under indoor climate conditions to provide frying temperatures of 170-180°C for the oil. The tested items revealed that the frying time for 250 g potato chips is 17 min, while rice takes 20 min to be cooked in each batch. In another attempt conducted by Geddam et al. [40], a finned SBC coupled with paraffin as the PCM was numerically investigated. Results demonstrated that the fined structure increases the heat transfer and reduces cooking time, while PCM brings consecutive cooking and keeps foodstuffs hot for 3-4 h.

The integration of selective surface showed benefits for SBCs where Cuce [41] presented a novel micro/nanoporous absorber for a cylindrical solar cooker. It showed a significant improvement in the absorber temperature and the air temperature as 24.1°C and 42.8°C, respectively. Ghosh et al. [42] tested a SBC incorporated with a glass cover coated with antimony doped indium oxide (IAO) to reduce emissivity and increase thermal insulation.

Results indicated that the coated single glass performs the same as a double-glazed cooker while suggesting lower cost and weight with higher durability.

Recently, several researchers such as Jang et al. [43], Al-Shamaileh [44], and Shanmugan et al. [45] have proposed several coatings to be applied on absorber plates using different nanomaterials. Bhavani et al. [46] used fuzzy rules to study the performance of a simple SBC in which the absorber was coated with nanoparticles (Al_2O_3). It was found that the proposed model can provide an excellent presentation for heat transfers to take place inside the cooker. Palanikumar et al. [47] also developed a simple BSC coupled with PCM and coated by Al_2O_3 nanoparticles and analyzed its performance using fuzzy logic and thermal image processing techniques. Results indicated that in the case of egg boiling, the overall efficiency is enhanced by 15.41%.

In this study, a thorough investigation has been conducted on three SBCs as SBC with PCM, with NPCM, and without NPCM (also known as the conventional solar cooker (CSC)) to improve the internal heat transfers resulting in higher heat generation. In this regard, synthesis and characteristics of $MgAl_2O_4$/Ni-doped, Fe_2O_3 nanomaterials, and PCM (waste cooking oil and $C_4H_4O_3$) suitable for use in solar cookers have been studied and analyzed. A simulation model was also developed using intelligent fuzzy logic and Cramer's rule where parameters of the temperature of glass covers (1 and 2), the temperature of the bar plate, the stuffiness of the cooked food, and the internal air temperature of the cooker were verified with experimental data. The thermal image processing technique was also implemented to evaluate the stuffiness of the cooked food given thermography performance i.e., in terms of temperature.

2 Material and methods

2.1 Cooker design

A layout of three designs of the same SBCs (i) with NPCM, (ii) with PCM, and (iii) without NPCM (CSC) are depicted in Fig.1(a). The proposed cookers designed based on terms of the model proposed by El-Sebaii and Ibrahim [48], and Nahar [49], where in their designs, the solar cooker consisted of an inclined double-glass cover, bar plate absorber coated with $MgAl_2O_4$/Ni-doped, Fe_2O_3 nanocomposite, copper coils filled with PCM, a plywood structure, and a cooking vessel. To increase solar energy absorption by the SBC as demonstrated by Algifri and Al-Towaie [50], two glass sheets with 4 mm thickness and a 0.02 m gap were used to form a 1 m^2 aperture area.

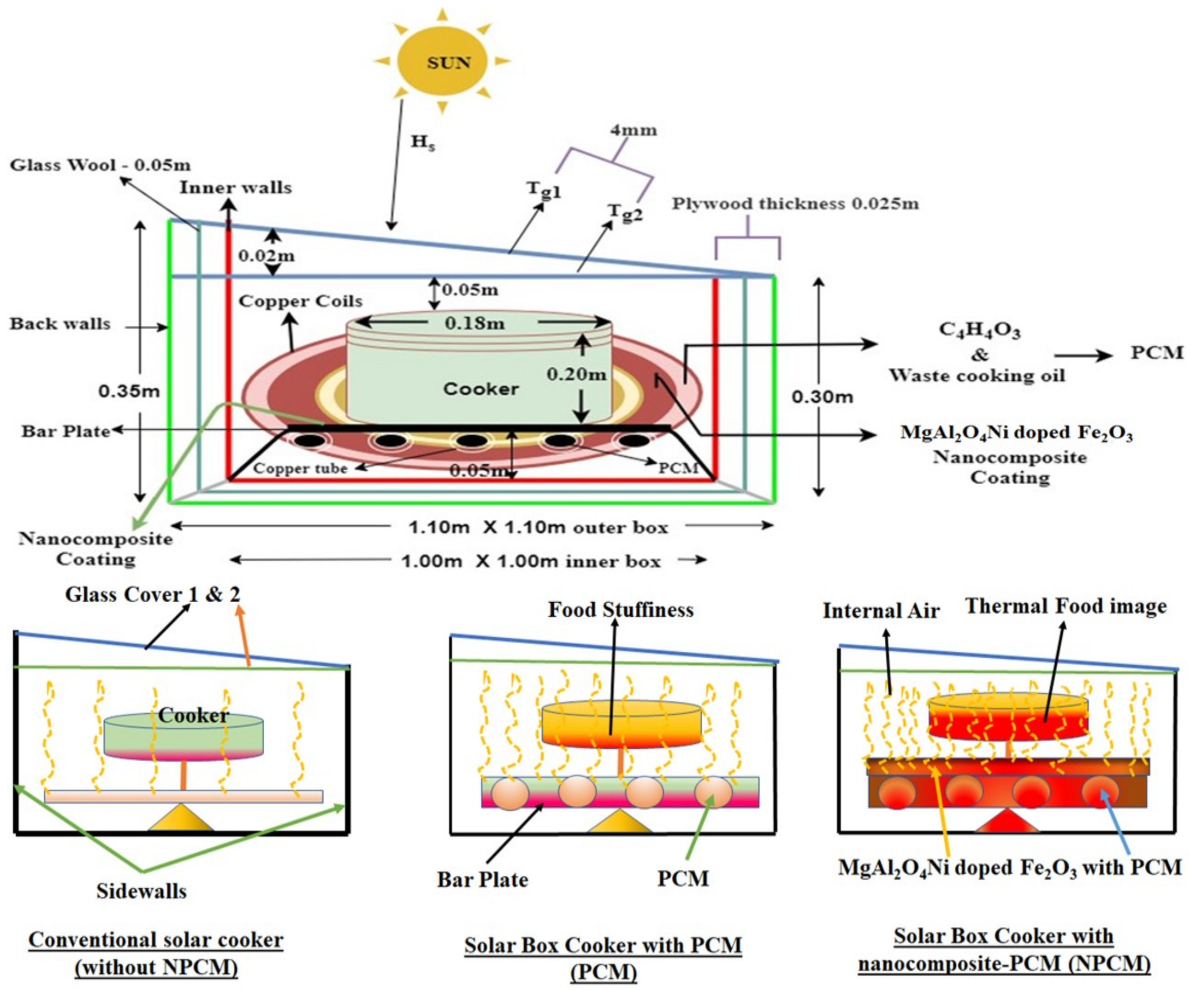

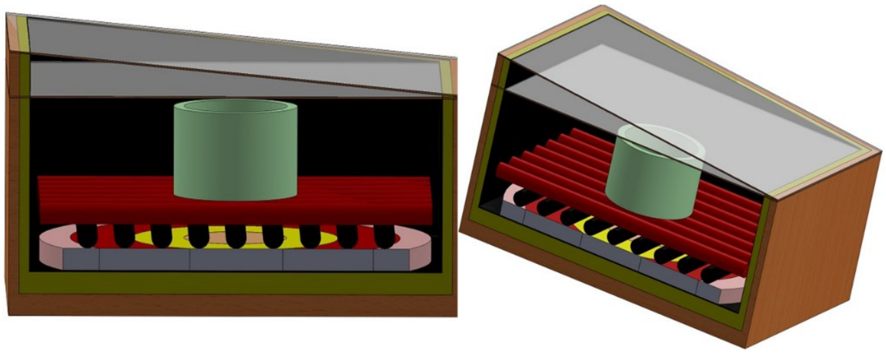

3D view of the solar cooker with NPCM

Figure 1. (a) Schematic illustration of three SBCs with the same dimension (i) without NPCM (CSC) (ii) with PCM, and (iii) with NPCM, (iv) 3D design of the solar cooker with NPCM.

The cooker structure was made of plywood because of its low fabrication costs, higher availability, improved solidity, and sufficient endurance under test conditions. In this regard, five plywood surfaces with 0.025 m thickness were used to form the cooker structure with outer dimensions of 1.10 × 1.10 m with a height of 0.30 m (front side) and 0.35 m (outer-back wall). The losses from the cooking surface reduced the available thermal energy. The plywood structure was correctly sealed and wrapped from sidewalls and cooker bottom using the glass wool with 0.05 m thickness. It is followed by the heat transfer process presented by Kumar [51].

Inside the cooker, an aluminum cylindrical cooking vessel with a lid diameter of 0.18 m and a height of 0.20 m placed over the absorber plate with a 0.05 m gap beneath the glass cover. The bar plate absorber was also fixed at the bottom of the cooker with 0.05 m height to make enough PCM space installation. Although Algifri and Al-Towaie [50] suggested an aluminum absorber plate in their work, in the presented work, the copper sheet was selected and used due to its higher resistance to corrosion, flexibility, elasticity, hygienic, and smoothness features. The absorber plate was coated with $MgAl_2O_4$/Ni-doped, Fe_2O_3.

2.1 Experimental setup

Three proposed SBCs were designed, simulated, and investigated at the Department of Physics, Center of Nanotechnology and Renewable Energies Development, Vijayawada, Southeast Indian state of Andhra Pradesh (16.5062 °N, 80.6480 °E). An experimental evaluation of the novel cooker carried out from January 2019 to February 2020, performing a set of outdoor tests measuring the effects of the proposed configuration on a set of parameters, including:

(i) Ambient temperature (T_a),

(ii) Fluid temperature inside the vessel (T_f),

(iii) Internal air temperature (T_{ina}),

(iv) Glass covers' (1 and 2) temperatures ($T_{G\ 1,\ 2}$),

(v) Absorber plate's temperature (T_{bp}),

(vi) Solar radiation (H_s), and

(vii) Wind speed (w_s).

Measuring all parameters including solar radiation, ambient temperature, and wind speed were carried out in 30 minutes. Fig.1(b) (A, B, C, D) illustrates the experimental setup developed in this study where the wind speed (m/s) was measured using an anemometer (WSSw/AVO) with a testing range of 0.5-50 m/s. Kipp and Zonen's CMP21 pyranometer was used to measure solar irradiance (W/m²). Also, temperatures of different components were measured using thermocouple wires and a digital multimeter. The ambient temperature (°C) was measured using camp bell CS215.

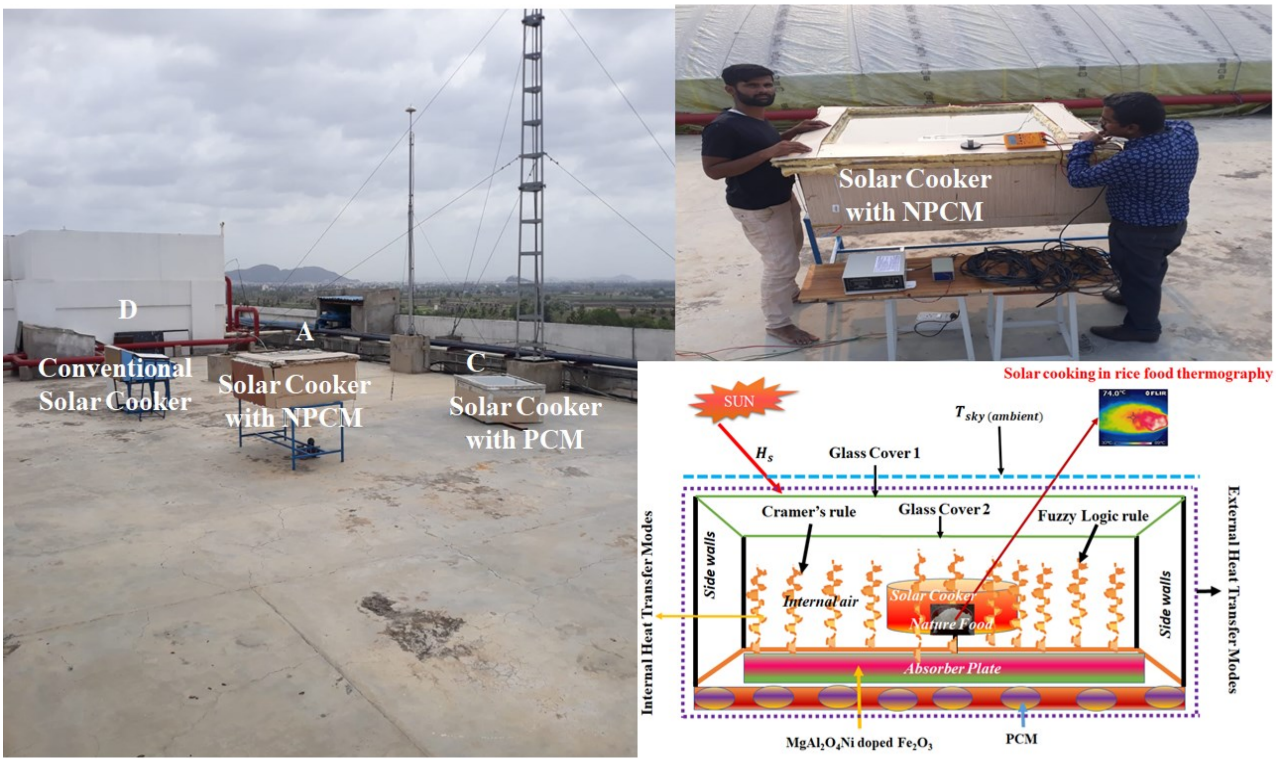

Figure 1. (b) (A, B – internal process, C, D) the experimental setup of SBCs (i) with NPCM (ii) with PCM, and (iii) without NPCM (CSC).

2.2 *Integration of PCM*

A bar plate absorber was fixed at the bottom side of the cooker and the PCM was integrated with the cooker through the coiled copper pipe with an inner diameter of 1.5 mm. The lower copper coils (at the bottom side) were filled with 3,000 g PCM composed of waste cooking oil and stearic acid ($C_4H_4O_3$). The bar plate was fixed inside the solar cooker and below ten copper pipes. It was placed inside 1,500 g of PCM to support the cooker (Fig. 2b (A) - NPCM). The main benefits of the proposed PCM are high specific heat, improved chemical stability, reversible freeze-melt cycle, low cost, large-scale availability, and high compatibility with NPCM. The effectiveness of PCM integration for solar cookers was tested under both loaded and unloaded conditions. It was shown that the mixture of $C_4H_4O_3$ and waste cooking oil (PCM) has a considerable capability to store thermal energy in a long-time process, where the absorber's temperature remains constant during the operating time. The mixture of $C_4H_4O_3$ and waste cooking oil as the PCM intensifies the natural convection heat transfer. In this way, the solar energy is absorbed by cookers where the heat flow is from the absorber plate to the PCM until it reaches the melting point. When the PCM melts, the cooker absorbs excess thermal energy which is stored as sensible heat. The NPCM employs the latent heat of $C_4H_4O_3$ and the waste cooking oil (PCM) to increase the absorbtion of solar radiation. Therefore, the PCM brings an additional thermal power source in nocturnal operations or cloudy and cold periods when solar radiation is not available or sufficient [52]. The amount of thermal energy absorbed by the bar plate absorber and is stored in the PCM (Q_{pcm-bp}) can be obtained as:

$$Q_{pcm-bp} = \int m_{bp} C_{bp} dT = mC_{av}(T_i - T_f) \tag{1}$$

The bar plate absorbs a fraction of the solar radiation used to increase the temperature of the PCM. The plate absorber's total amount of heat transfer is:

$$Q_{f-bp} = a_f m \Delta h_c \tag{2}$$

2.2.1 The PCM characteristics

The mixture of $C_4H_4O_3$ and waste cooking oil (PCM) improved viscosity and maintained a temperature of 50°C for the system. The thermal energy storage at the temperature of 137°C by the PCM was reported by Oturanç et al. [53] and Buddhi et al. [54]. The cooking waste oil was collected from the Koneru Lakshmaiah Education Foundation (KLEF) hostel in March 2019, with thermo-physical characteristics presented in Table 2. The mixture of $C_4H_4O_3$ and waste cooking oil (PCM) can transmit the sunlight and provide a melting point of 35-60°C. Since the PCM-based thermal energy systems utilize the latent heat from melting or freezing phenomena, the energy stored by the solid to liquid phase change is at least 1-2 orders of magnitude higher than that of stored through sensible heat storage with a 10°C temperature difference. During the phase change process, the PCM can absorb the coming heat while its temperature remains steady for a while. Thus, the energy gained by $C_4H_4O_3$ and waste cooking oil is in the forms of the latent heat of fusion from solid to liquid. The high values of fusion latent heat indicate that the proposed PCM could store a considerable amount of heat through the phase transition while its temperature remains constant near the melting point. As a result, this system can be a good option when short-time cooking applications are considered. Table 1 summarizes the PCM properties in the same procedure reported by Jin and Zhang [55]. As Table 2 represents, three standard test conditions measuring the time requirements for the PCM to reach the absorber's temperature from its melting point.

Table 1. Thermo-physical properties of $C_4H_4O_3$ and waste cooking oil (PCM).

Properties	**$C_4H_4O_3$**	**Waste Cooking Oil**
Melting temperature (T_m) - (°C)	119 to 120	32 to 37
Thermal conductivity (K_s) - (W/mK)	0.29	0.168
Specific heat (C_p) - (kJ/kgK)	1.2340	1.67
Latent heat of fusion (L_{pcm}) - (kJ/kg)	134.0	250
Density (ρ_s) - kg/cm^3	1.234	0.91 to 1.0
Refractive index	1.476	1.4719–1.4740
Vapor density (vs air)	7.38 to 8.63	7.7

Table 2. Standard time characteristics obtained as a function of the absorber's temperature.

Test condition	**Absorber's temperature**	**Time**
Lower - T_{bp}	95 ^{0}C	35 min
Middle - T_{bp}	110 ^{0}C	45 min
Higher - T_{bp}	137 ^{0}C	60 min

2.3 Integration of nanocomposite coating

Synthesis of $MgAl_2O_4/Ni/Fe_2O_3$

The MoS_2-Fe_2O_3 film was developed through an electrodeposition method reported by Cong et al. [56], Wang et al. [57], and Cong et al. [58]. The nanocomposite powders' preparation was carried out by dissolving 0.130 g of $MgAl_2O_4$ and 0.126 g of Fe_2O_3 in 85 mL of distilled water. Then, $MgAl_2O_4$-Ni material was added to a 27 mL solution of the precursor. Additionally, Fe_2O_3 solution (91.35g) was mixed with distilled water and placed in the magnetic stirrer to form the equal growth of composite materials. Then, to make the powder, the product was dried and consequently deposited into the solution using an electrophoretic method at a given time at a constant voltage of 4.0 V. Finally, the $MgAl_2O_4$/Ni/Fe_2O_3 film was applied to the uncoated plate absorber of the SBC to improve the solar absorption and the operating temperature.

2.3.1 Nanocomposite coating characteristics

Fig.2(a) graphically shows the steam iron method and decomposition of the environment control. The crystalline segments of the $MgAl_2O_4$/Ni/Fe_2O_3 were determined using X-ray diffraction (XRD), as shown in Fig.2(b). The central peak was at 2θ of 36.5°, corresponding to 311 planes using a Phillips PANalytical X'PERT diffractometer. The nanocomposite characterized the use of X-ray photoelectron spectroscopy to control the valance states. The atomic crystal compositions are consistent with the C1s maximum (282.4 eV). The absorption coefficient up to the range of 10^4 cm^{-1} was obtained. Fig.2(c) shows the morphology of $MgAl_2O_4$/Ni/Fe_2O_3 in the process of production using Hitachi Model S-4700 (II) Scanning Electron Microscopes (SEM). The SEM morphology was followed by an experimental band gap of 1.5 eV for $MgAl_2O_4$/Ni/Fe_2O_3 materials as illustrated in this figure. Some formations such as (A) Ni/Fe_2O_3 nanosheets, (B) Fe_2O_3/ $MgAl_2O_4$ composite, and (C) $MgAl_2O_4$/Ni/Fe_2O_3 were obtained. The SEM analysis of composite material revealed the average size of molecules between 0 to 20 μm.

Fig.2(d) shows EDX elements analysis of the $MgAl_2O_4$ /Ni/ Fe_2O_3 (the element of red, green, and blue colors) that confirms the suitability of the absorption elements. The coating layer applied to the copper sheet was used to improve the internal heat transfer process of the proposed solar cooker. Therefore, the $MgAl_2O_4$ /Ni/ Fe_2O_3 material (Purity = 99.99 %) with a typical particle size of 0.5 μm (γ) and a density of 3880 Kg/m^3 were used in this design. Fig. 1(a) is a schematic diagram indicating the heat absorption mechanism that happens inside the cooker with the NPCM due to nanocomposite integration by [59].

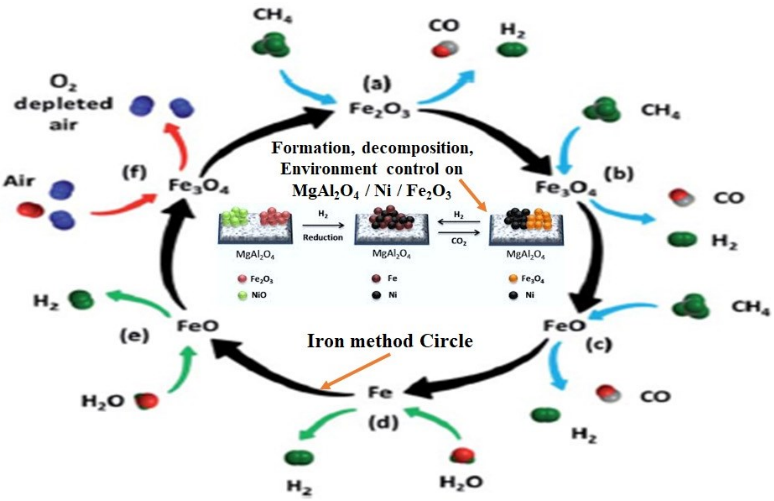

Figure 2. (a) Graphical representation of the Steam Iron method and decomposition environment control.

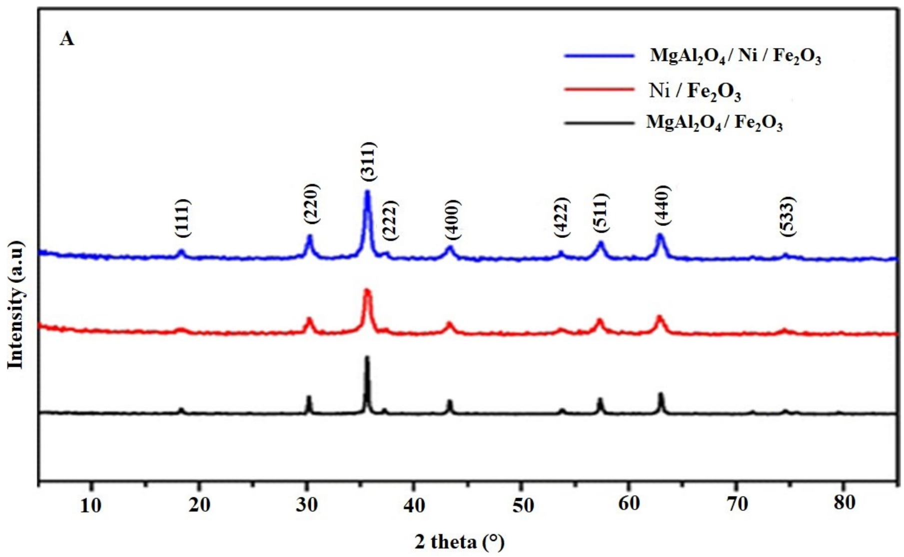

Figure 2(b). XRD patterns and SEM analysis of the MgAl2O4/Ni/Fe_2O_3.

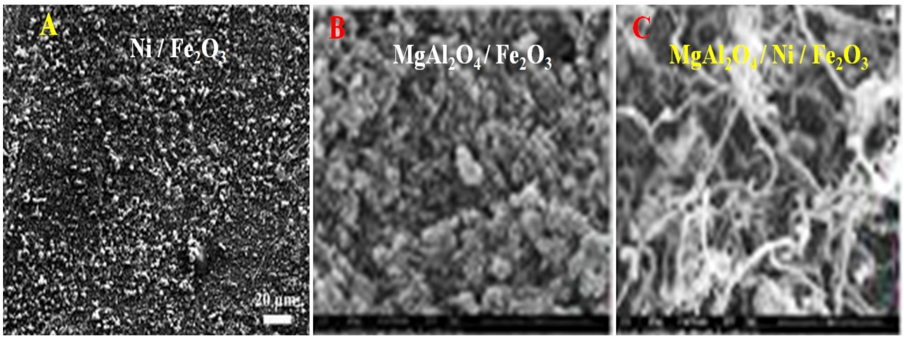

Figure 2(c). The SEM analysis of the $MgAl_2O_4$ /Ni/ Fe_2O_3.

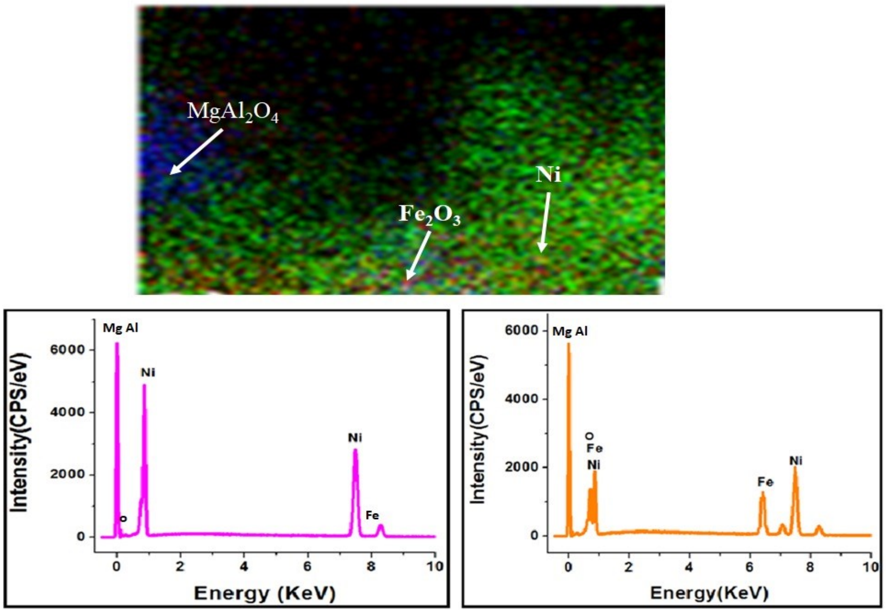

Figure 2(d). The EDX elements analysis of the $MgAl_2O_4$ /Ni/Fe_2O_3 (element of Red, green, and blue colors).

2.3.2 Solar spectrum reflectance/absorbance characteristics

The spectrophotometer was used to analyze the spectral reflectance and absorbance distributions with the wavelength of the nanocomposite materials. Fig.2(e) shows a solar spectrum spreading with colors of black (reflectivity), red (solar radiation), blue (transmissivity), and green (nanocomposites materials). Each color shows an increase of the wavelength of the image as for the green it is 0.5-10 μm, and for the red, it is 0.4-0.50 μm. The spectrophotometer measured the reflectance and absorbance of samples with two types of light as the first was ultraviolet-visible spectroscopy (UV-VIS) region and the second was IR. The

IR band was activated at 0.930 μm and UV-VIS finished at 1,503 nm, resulted in peak values in the band of 0.930 μm and modified an optical property of the nanocomposite's materials. The combination of nanocomposites material/PCM increased the IR fraction and the average reflection values.

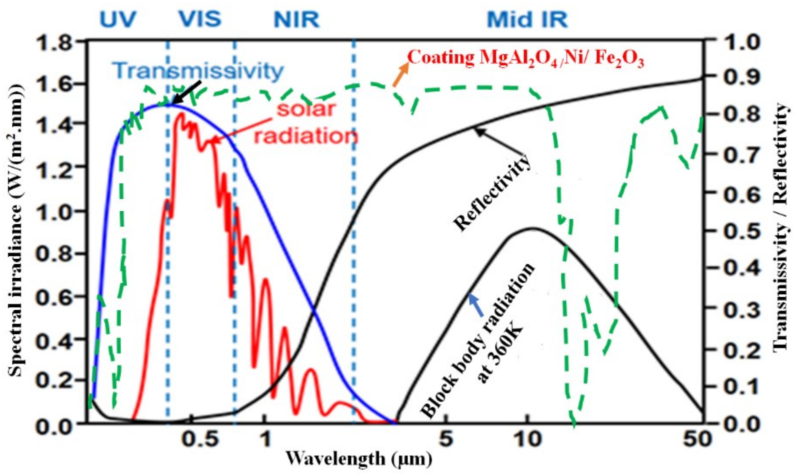

Figure 2(e). Analysis of solar spectrum reflectance/absorbance of the $MgAl_2O_4$/Ni/ Fe_2O_3 coating.

2.4 Fuzzy logic application

The fuzzy synthesis appraisal evaluated the NPCM by considering U and W as the Universe of factors and the Universe of appraisals, respectively. It can be written as;

$$U = \{U_1, U_2, ...U_n\} \quad (3)$$

$$W = \{W_1, W_2, ...W_m\} \quad (4)$$

If $F = \{f_{ij}\}$ is a fuzzy relation where $i = 1,2, ..., N$ and $j = 1,2, ..., M$, Table 3 represents the simple matrix for the developed fuzzy relations. The internal heat transfer process of the proposed design was evaluated in which a set of weights (W_i) assumed to be the factors of ambient temperature (T_a), solar radiation (H_s) W/m^2, fluid temperature (T_f), and wind speed (Ws). The convection weightage of the cooker for all parameters is presented in Table 4. Each of the proposed weights is a value of membership for each factor as U_i. It can be given as the fuzzy vector;

$$V = \{w_1, w_2, w_3, w_4, ... w_n\} \quad (5)$$

where $\sum_{i=1}^{n} W_i = 1$

According to the literature [60], the manufacturing specialists have made a specific weight for each parameter of a system, such as the ambient temperature (0.2), the intensity of solar radiation (0.7), and wind speed (0.1). The fluid temperature is a parameter for the NPCM, which has a weightage of 0.5 to form the factor *E*. To evaluate the performance of the system, each member of the evaluation categories needed as W_i given by:

- Reduction
- Idealistic (No change)
- Upsurge

Therefore, taking the NPCM integrated with internal heat transfer for the fuzzy analysis by the composition O as min-max composition operation of E and J can result in a relation, where the fuzzy vector S_p can be written as:

$$S_P = E \; O \; J \tag{6}$$

Implementing Eq. (6) leads to the following:

$$S_P = E \; O \; J$$

$$S_P = \max \{e_x, e_y, e_z\}$$

$$S_P = \max \{0.7, 0.1, 0.1\}$$

Where

e_x = Max {Min (0.2, 0.6), Min (0.7, 0.8), Min (0.5, 0.7), Min (0.1, 0.6)}

e_y = Max {Min (0.2, 01), Min (0.7, 0.1), Min (0.5, 0.2), Min (0.1, 0.3)}

e_z = Max {Min (0.2, 0.3), Min (0.7, 0.1), Min (0.5, 0.1), Min (0.1, 0.3)}

Table 3. The suitable values of different parameters affecting the NPCM.

Parameters	Reduction	Idealistic (No change)	Upsurge	Total Weightage
Ambient temperature (T_a)	0.6	0.1	0.3	1.0
Solar radiation (H_s)	0.8	0.1	0.1	1.0

Fluid temperature (T_f)	0.7	0.2	0.1	1.0
Wind speed (Ws)	0.6	0.3	0.1	1.0

Therefore, all categories are used for the outcomes of the fuzzy vector estimation. The fuzzy rules applied with IF and THEN for the cooker temperature on Reduction energy level, Idealistic energy level, and Up-surge energy level. Fig.3(i) represents the fuzzy structure of food stuffiness (fluid) based on the principle of fuzzy logic. In this regard, it would be suitable if the solar radiation is higher than fluid (cooking materials -rice). The following rules are shown for the NPCM.

(i) IF Ambient Temperature (T_a) AND Solar radiation (H_s) Upsurge, THEN Food stuffiness Upsurge.

(ii) IF Solar radiation (H_s) AND Fluid Temperature (T_f) Reduction, THEN Food stuffiness Reduction.

(iii) IF Fluid Temperature (T_f) AND Wind Speed (W_s) are Idealistic, THEN Food stuffiness is Idealistic.

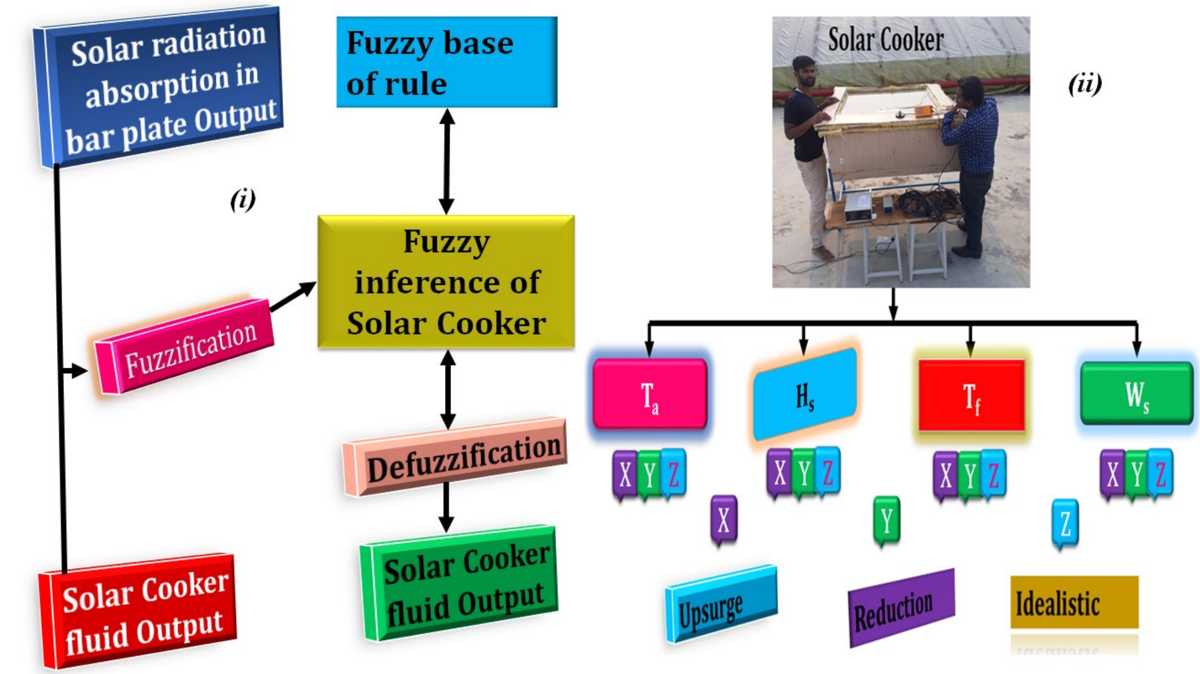

Figure 3. (i & ii) Control Fuzzy rules for the cooker in food stuffiness yielded by the NPCM.

Table 4. Characterization of the fuzzy relation of the NPCM.

	W_1	W_2	…	W_M
U_1	f_{11}	f_{12}		f_{1M}
U_2	f_{21}	f_{22}		f_{2M}
.	.	.	.	.
U_N	f_{N1}	f_{N2}		f_{NM}

2.4.1 Performance of nanocomposite coated on bar plate

The NPCM absorbed by the solar cooker was stored for the heat transfer fraction process by applying fuzzy logic rules for renewable energy sources. The fuzzy rules were developed based on heat transfer upon overall fuzzy inputs and outputs of the system. They evaluated the NPCM performance for the parameters such as U_1 = ambient temperature, U_2 = solar radiation, U_3 = fluid temperature, and U_4 = wind speed, as shown in Fig.3(ii). The productivity of the NPCM was determined considering the factor T_a as 0.35, H_s as 0.680, T_f as 0.71, and W_s as 0.3. The result of "*E*" was implemented for all solar cooker factors from equation (6). Composition delivered by S, while the estimation vector functions selected as the uppermost membership in the group "Upsurge".

In Figs.3 (iii, iv, and v), the solar cooker indicates that the membership functions are the *Ta*, *Hs*, inputs, and outputs' convective energy method. The application of the fuzzy logic rules carried out with the implementation of the fuzzy logic toolbox. The membership functions formed, where their sum was on the entire interval of 1. The variation of the temperature for the NPCM is equal to membership functions representing along the axes (x, y).

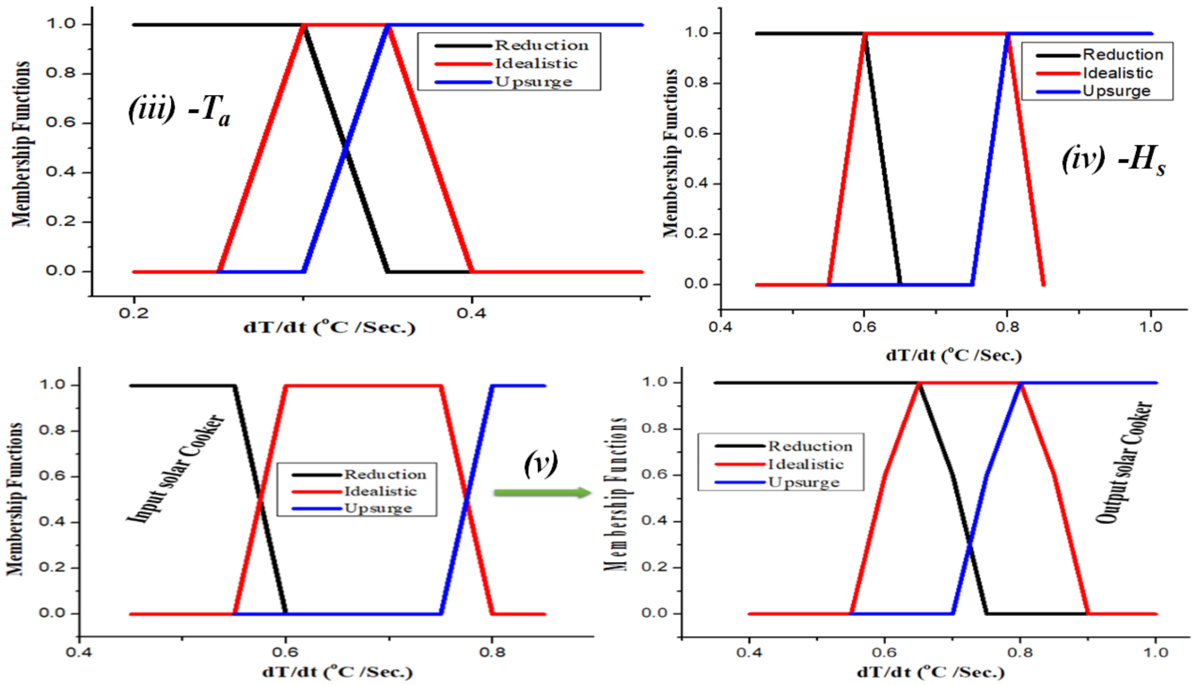

Figure 3. (iii, iv &v) Fuzzy logic Membership functions for T_a, H_s, and input and output control of the cooker.

2.5 *Thermal modeling*

The fuzzy rule applied for the thermal image processing assisted in the model of the proposed cooker's thermal behaviors, as shown in Fig.4(a). Therefore, to evaluate the cooker's performance, several energy balance equations were developed for different components like the bar plate absorber, cooking vessel, cooking fluid, internal air, and upper and lower glass covers. In this study, the following assumptions are applied to simplify the modeling equations:

1. The amount of solar radiation stored by the cooker's components is neglected.
2. The internal heat transfer coefficients are developed based on constants.
3. The total solar energy absorbed by the cooker elements, including the bar plate, sidewalls, vessel, and lid, is perfectly transferred to NPCM through conduction.
4. The total energy loss from the NPCM to the ambient neglected
5. The distance used for the heat conduction from the bottom side of the bar plate is equal to the thickness of glass covers (4 mm).

The energy balance equation on the first cover

The first cover absorbs a fraction of solar radiation that reaches the aperture of the NPCM. In contrast, the heat transfer to the second cover occurs through the convective and radiative heat transfer processes.

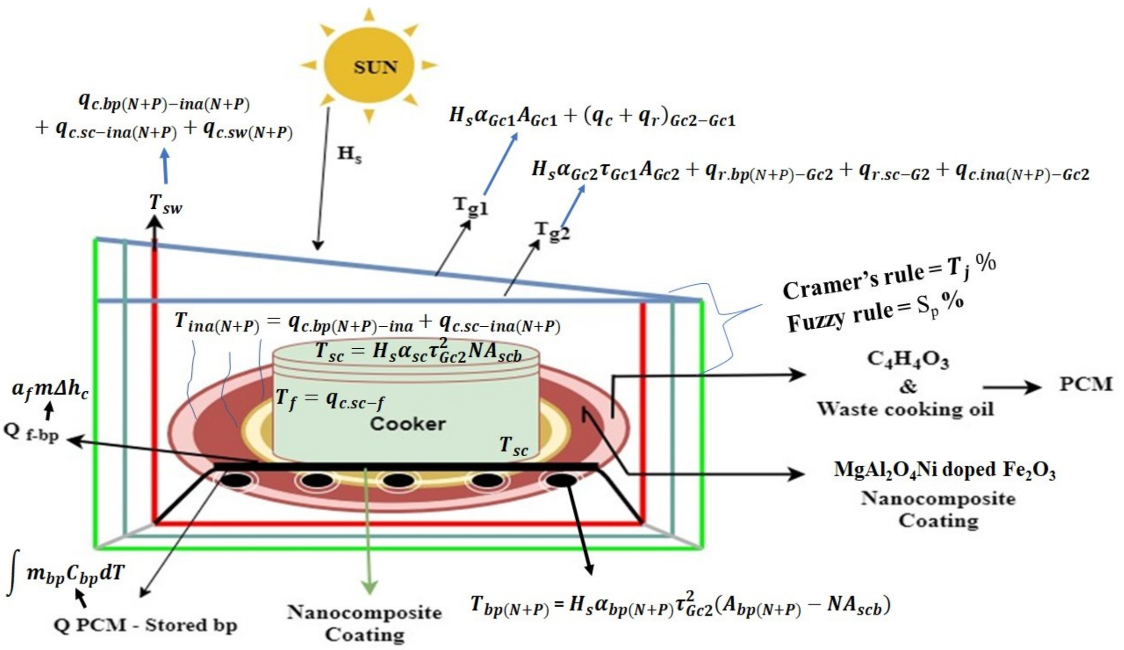

Figure 4. (a) Schematic of the heat transfer process in the NPCM.

The amount of energy absorbed by the glass cover will be lost through the radiation and convection to the sky and ambient, respectively. As a result, the energy balance equation for the cooker can be stated as:

$$(mC_p)_{Gc1}\frac{dT_{Gc1}}{dt} = H_s\alpha_{Gc1}A_{Gc1} + (q_c + q_r)_{Gc2-Gc1} - q_{r.Gc1-sky} - q_{c.Gc1-Amb.} \quad (7)$$

The energy balance equation on the second cover

The heat was absorbed by the lower glass cover (II) from the plate absorber and the cookers's inside air. Simultaneously, the solar radiation was transferred from the upper glass to the lower glass cover through the convection process. Therefore, the energy balance equation on the glass cover-II can be expressed as:

$$(mC_p)_{Gc2}\frac{dT_{Gc2}}{dt} = H_s\alpha_{Gc2}\tau_{Gc1}A_{Gc2} + q_{r.bp(N+P)-Gc2} + q_{r.sc-G2} + q_{c.ina(N+P)-Gc2} - q_{c.Gc2-Gc1} - q_{r.Gc2-Gc1} \quad (8)$$

The energy balance equation on the internal air

The internal air absorbs heat from the cooker's plate absorber by convection and losses to the lower glass cover through convection. Therefore, the energy balance equations can be written as:

$$(mC_p)_{ina(N+P)}\frac{dT_{ina(N+P)}}{dt} = q_{c.bp(N+P)-ina(N+P)} + q_{c.sc-ina(N+P)} - q_{c.ina(N+P)-Gc2} \quad (9)$$

The energy balance equation on side walls

The side walls gain heat from an internal air through a convection process in which heat is transferred from the absorber plate to the side walls while there is a heat loss to the lower glass cover. The energy obtained by the side walls can be written as:

$$(mC_p)_{sw}\frac{dT_{sw}}{dt} = q_{c.bp(N+P)-ina(N+P)} + q_{c.sc-ina(N+P)} + q_{c.sw(N+P)-ina(N+P)} - q_{c.ina(N+P)-sc} - q_{c.ina(N+P)-Gc2} \quad (10)$$

The energy balance equation on the cooking vessel

Inside the NPCM, a portion of the transmitted solar energy is absorbed by the cooking vessel containing the cooking fluid that also receives thermal power from the absorber. In this process, the vessel transfers a portion of the absorbed heat to the cooking fluid as the convection process. Simultaneously, the remaining energy is lost by the internal air and the inner glass cover in the forms of convection and radiation, respectively. Thus, the energy balance equation of the cooking vessel can be expressed as:

$$(mC_p)_{sc}\frac{dT_{sc}}{dt} = H_s\alpha_{sc}\tau_{Gc2}^2 NA_{scb} + q_u - q_{c.sc-f} - q_{r.sc-Gc2} - q_{c.sc-ina(N+P)} \tag{11}$$

The energy balance equation on the cooking fluid

The thermal energy transferred from the solar cooker to the cooking fluid as a convection heat transfer can be written as:

$$(mC_p)_f\frac{dT_f}{dt} = q_{c.sc-f} \tag{12}$$

The energy balance equation of the absorber plate

The absorber plate receives solar energy and becomes hot, providing useful energy to the vessel. However, a portion of the absorbed energy is lost by the internal air and the inner glass through convection and radiation as following:

$$(mC_p)_{fbp(N+P)}\frac{dT_{bp(N+P)}}{dt} = H_s\alpha_{bp(N+P)}\tau_{Gc2}^2(A_{bp(N+P)} - NA_{scb}) - q_u - q_t - q_{r.bp(N+P)-Gc2} - q_{c.bp(N+P)-ina} \tag{13}$$

where $u_b = \frac{k_b}{x_b}$ is the minimum heat loss-coefficient of the proposed NPCM and can be determined using equations (7) to (13) as following:

$$A_1T_{Gc1-Gc2} + B_1T_{ina(N+P)} + C_1T_{bp(N+P)} + D_1T_{sc} = S_{Gc1-Gc2} \tag{14}$$

$$A_2T_{Gc1-Gc2} + B_2T_{ina(N+P)} + C_2T_{bp(N+P)} + D_2T_{sc} = S_{ina(N+P)} \tag{15}$$

$$A_3T_{Gc1-Gc2} + B_3T_{ina(N+P)} + C_3T_{bp(N+P)} + D_3T_{sc} = S_{bp(N+P)} \tag{16}$$

$$A_4T_{Gc1-Gc2} + B_4T_{ina(N+P)} + C_4T_{bp(N+P)} + D_4T_{sc} = S_{sc} \tag{17}$$

The temperatures of the double-glass glazing that covers the NPCM were achieved using the coefficients of A, B, C, D, and S where the integration of Cramer's rule makes equations (14) to (17) as:

$$T_j = \frac{\Delta_j}{\Delta} \tag{18}$$

Here, j used an index to represent double glass covers, internal air, cooking vessel (fluid), and absorber bar plate, while Δ is a factor for the thermal coefficients used in equations (7) to (13), and Δ_j is a factor obtained by substituting the thermal coefficients of T_j by S in equations mentioned above. Thus, it can be written as:

$$\Delta = \begin{vmatrix} A_1 + B_1 + C_1 + D_1 \\ A_2 + B_2 + C_2 + D_2 \\ A_3 + B_3 + C_3 + D_3 \\ A_4 + B_4 + C_4 + D_4 \end{vmatrix} \tag{19}$$

Two glass covers evaluated in temperature using the following equations derived from equation (18) as:

$$T_{Gc1\,-\,Gc2} = \frac{\Delta_{Gc1\,-Gc2}}{\Delta} \tag{20}$$

$$T_{ina} = \frac{\Delta_{ina}}{\Delta} \tag{21}$$

$$T_{bp} = \frac{\Delta_{bp}}{\Delta} \tag{22}$$

$$T_{sc} = \frac{\Delta_{sc}}{\Delta} \tag{23}$$

Having $A = \frac{K_g m_{k_g} + K_p m_{k_p} + K_i m_{k_i}}{\Delta}$ and $N = m_{kt}/\Delta$, where *m* is insignificant of K_i. The relation can be derived from equation (18):

$$T_{sc} = A - NK_f T_f \tag{24}$$

Substituting T_{sc} from equation (24) into equation (11), it can be given as:

$$f(t) - aT_f = x\left(\frac{dT_f}{dt}\right) \tag{25}$$

where *a* and *f(t)* are functions of the solar intensity, ambient temperature, and different heat transfer coefficients, conducting several calculations, a, *f(t)*, and x were found to be:

$f(t) = AT_f,\ a = K_f\ (1 + K_f)$ and $x = m_f\ C_f$

The values of the double glass covers are substituting in equation (25), it can be obtained as:

$$T_{f-N+P} = \frac{F(t)_{av}}{a}\left[1 - e^{\left(-\frac{at}{x}\right)} + T_{int}e^{\left(-\frac{at}{x}\right)}\right] \quad (26)$$

Here, T_{int} is the initial temperature of the cooking fluid, $F(t)_{av}$ is the average value of f(t) over the infinitesimal time interval from 0 to t is assumed to be constant values. Thus, equation (26) calculated the cooking fluid temperature and equations (7) to (13) were used to calculate the temperature values of the other components.

The integration of nanoparticles is used to increase the system's absorbed energy, resulting in higher quality output. Internal energy with a performance of an NPCM is occupied as cooker follows;

$$E_{o\text{-}N+P} = \frac{m_w C_w\left(T_{f\text{-output}} - T_{f\text{-input}}\right)}{A_c H_S t} + \frac{u(T - T_a)}{H_s} \quad (27)$$

where the amount of total energy ($Q_{total\ energy\ +\ (N+P)}$) absorbed by the NPCM-coating can be written as:

$$Q_{total\ energy\ +(N+P)} = \frac{E_o\ .\ \Delta T_{\infty}\text{-}95}{\Delta t} \quad (28)$$

Also, for calculating the total evaporation power ($\dot{Q}_{ep}$) exerted by NPCM, the following relation can be used as a function of cooking material and fluid temperature:

$$\dot{Q}_{ep} = Q_{total\ energy\ +N+P}\ .\ h_L \quad (29)$$

The overall thermal efficiency of the NPCM was evaluated as:

$$\eta_{\ total\ energy\ +(N+P)}(\%) = \frac{\dot{Q}_{ev}}{H_s\ .\ A_c} \quad (30)$$

Where the bar plate’s temperature with NPCM was verified using the intelligent rules as;

$$S_p\ (\%) = \eta\ (\%) \tag{31}$$

2.5.1 Thermal image processing

The thermal imaging method heated detected regions with temperature distribution upon an object. An infrared (IR) radiation technique emitted radiation from any item with a surface temperature above absolute zero is captured by a thermal camera. Thermal imaging evaluated the amounts of the thermal energy absorbed by different components of the cooker. Fig.4(b) shows the developed NPCM used during the experiments which can reach an operating temperature of 93 ºC, where the measured ambient temperature is 39 ºC. The other corresponding temperatures, such as H_s $T_{bp+(P+N)}$, $T_{G\,1,2}$, T_f, T_{ia+P+N} were also determined using the same procedure. The fluid cooking process was illustrated using thermography techniques, where the temperature of the food material is characterized by a bright yellow color (higher-temperature) to dark blue color (lower-temperature).

In the experimental tests (Fig.4b(A)), three different (Low, Middle, High) levels of the operating temperature for the boiled rice (Figs.4b (B, C & D), as low (Fig.4b(E)), middle (Fig. 4b(F)), and high (Fig.4b(G)) temperature thermographies were evaluated.

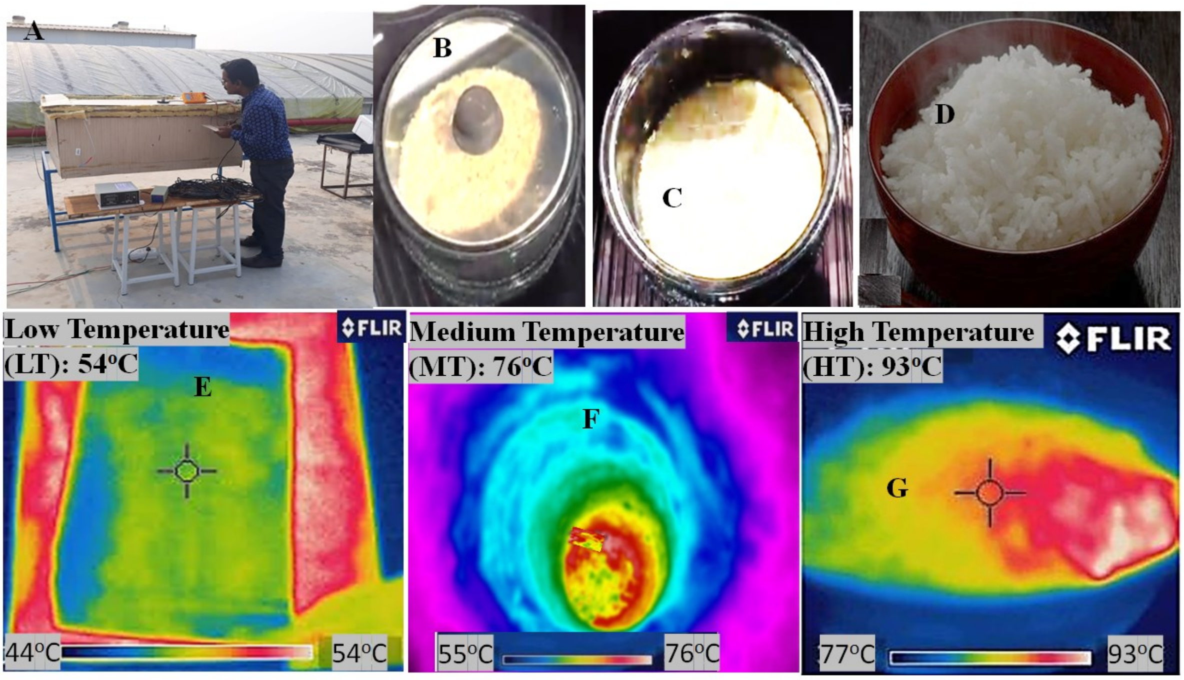

Figure 4(b). Illustrations of the real solar rice cooker and thermal images of the cooking process, image G adapted from [73].

The image segmentation approach has demonstrated many advantages over the other watershed transforms including simple, intuitive, and easy detection and segmentation. However, over-segmentation is the principal disadvantage of the watershed transform which decreases its indication-based process developed in the system by Palanikumar et al. [47]. The system verified the cooking materials' (rice) heat form of the image segmentation method. Since image segmentation is a powerful tool for watershed transformation, implementing this technique with MATLAB digital image processing can be a promising way to show the effects of the proposed modifications on the boiling rice.

2.5.2 Algorithm analysis

The watershed transform algorithm was implemented for the analysis of the food materials as thermal images. Fig.4(c) depicts the flowchart explaining the watershed algorithm used in this study.

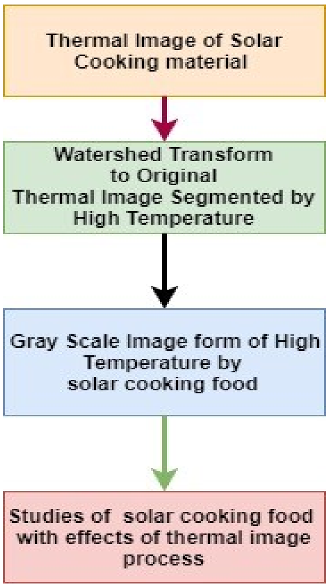

Figure 4(c). Flowchart diagram of the thermal image processing used for thermal images.

2.11 Segmentation of the cooking process images

Generally, segmentation is achieved by distinguishing the object's boundaries inside an image using pixel-level properties such as the texture, shape, edge, etc. The segmentation technique was performed on the cooking rice images based on faster analysis instructions reported in the literature [61]. Thus, three different segmentation techniques, including (i) Threshold segmentation, (ii) Edge Detection segmentation, and (iii) Region-based segmentation, were used in this study.

(i) **Thresholding Segmentation (G_s)**

The threshold segmentation algorithm was used to extract the boundaries inside the images, include cooking material with a contrasting background. The results were expressed in the form of a binary output derived from greyscale images. As a result, each thermal image defined as solar cooking temperature $T_{i\,s\,t}$(x, y), and the threshold images G_s(x, y) can be defined as following where $T_{i\,v}$ is the threshold image value:

$$G_s = (x, y) = 1, T_{i\,s\,t}(x, y) > T_{iv}, \qquad 0, T_{i\,s\,t}(x, y) < T_{i\,v} \tag{32}$$

(ii) **Edge detection for image segmentation**

Edge detection techniques allow the extraction of edges based on the changes in grey tones of images. In this regard, as continuity and end, two common factors can lead to the identification of edges. Therefore, the integration of this transformation results in edge image determination while not influencing the main image [62]. The fuzzy-based application to the membership function has determined a different way of heuristics (basics) in literature [60,63] where a new edge detector developed for the cooking image as:

$$\mu_{Edge-food}\left(\boldsymbol{G_s}(x,y)\right) = 1 - \frac{1}{1+\frac{\Sigma_n \|\boldsymbol{G_s}(x,y)-\boldsymbol{G_s}(i,j)\|}{\Delta}} \quad (33)$$

(iii) **Region-based segmentation**

Region-based segmentation has been observed in thermal image processing as spatial clustering. This technique uses two algorithms, namely **(a)** Region Merging and **(b)** Region Splitting as represented in equation (34):

$$\boldsymbol{\mu_{rb-F} = \Sigma i\,(x,y)\,/\,N} \quad (34)$$

(a) Merging area of cooking material

The rice's performance followed even up to a suitable seed area, and the image (rice boiling) strips on 2×2 or 4×4 blocks.

(b) Splitting area of food performs:

The flowchart diagram of a SBC absorbed heat energy production is shown in Fig.4(c). It uses splitting processes in the form of a decomposition system at the split/merge process stage.

2.5.3 Simulation of the solar cooker

The experiments were used to verify the developed mathematical model. A coefficient applied to the energy flux is absorbed by the NPCM as [49]. The parameters required for the modeling of the solar cooker were taken from the values reported by Funk [64] and Harmim [65], then the simulation carried out using python software. The assumed properties used in the modeling calculation areas are:

$\alpha_g = 0.05, A_{sc} = 0.0293m^2, A_{bp} = 0.10m^2\ , m = 1kg, C_p = 4190\ jkg^{-1}K^{-1}, \alpha_{bp} = \alpha_{sc} = 0.91,\ U_b = 0.3\ Wm^{-2}K^{-1}$, and $K_p = 385m^{-1}K^{-1}$ (Copper sheet).

The heat transfer coefficients used in the modeling process are taken from the values calculated by Hussain et al. [66] and Algifri and Al-Towaie [50]:

$h_{cp-air} = 13.8Wm^{-2}K^{-1},\ h_{c\ sc-air} = 25.4Wm^{-2}K^{-1}, h_{cp-air} = 12.8Wm^{-2}K^{-1}, h_{cua} = 11.4Wm^{-2}K^{-1}, h_{c\ sc\ f} = 440.2Wm^{-2}K^{-1}, h_{rus} = 5.9Wm^{-2}K^{-1}, h_{rpl} = 9.2Wm^{-2}K^{-1}, h_{rscl} = 8.9Wm^{-2}K^{-1}$.

The initial temperatures of the solar cooker's components are considered to be equal to the ambient temperature.

3 Results and discussion

3.1 Results of solar cookers

Some experimental tests for SBCs with PCM, with NPCM, and CSC were carried out to evaluate the bar plate absorber's thermal behavior coated with and without $MgAl_2O_4/Ni/Fe_2O_3$ mixture nanocomposite-PCM. The experimental analysis of the NPCM's thermal performance was conducted on a typical summer day. The impact of nanocomposite materials was studied based on the storage of thermal energy which affects the system's overall thermal performance. The experiments were conducted from 10:00 am to 2:00 pm to evaluate the system's performance under different levels of solar radiation (H_s) for the days on 04.04.2019, 22.05.2019, 10.06.2019, and 03.07.2019. Figs.5(a, b, c, d) illustrate the measured values of solar radiation and ambient temperature (T_a) used to verify the mathematical model. As shown in these figures, for a typical day with scattered clouds sky, the solar radiation shows an increasing trend from 10:00 am to 12:30 pm, while as noon passes, solar flux follows a constant trend due to the clear sky. These figures also show that the solar radiation and ambient temperature values range from 650 to 1100 W/m^2 and 33.46 to 40.23°C, respectively from January 2019 to February 2020 with an average value of 797 W/m^2 and 37.05°C.

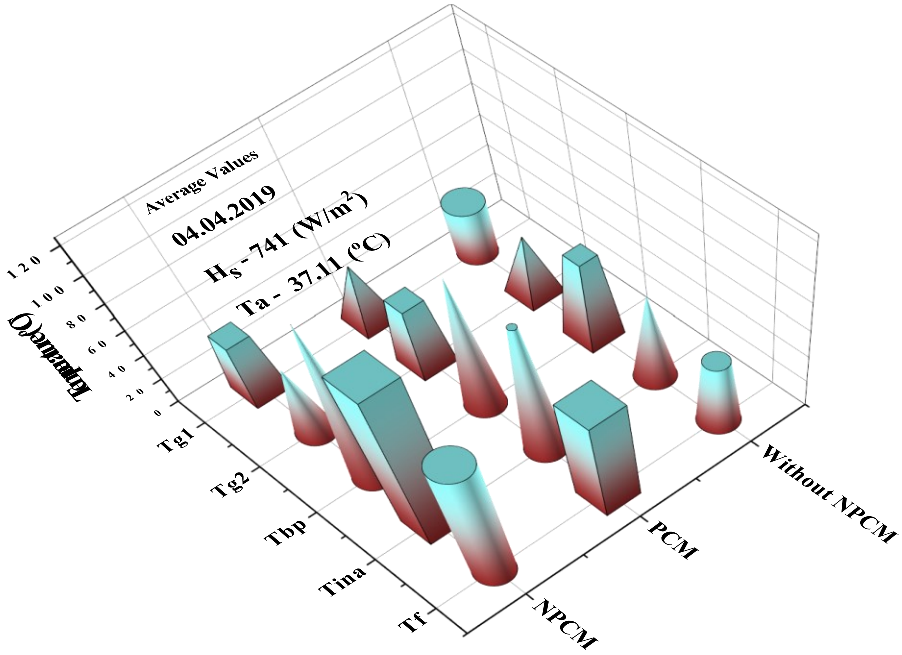

Figure 5(a). Variations of the average values of H_s, T_a, $T_{g1,2}$ T_{bp}, T_{ina} and T_f for SBCs (i) CSC (ii) with PCM (iii) with NPCM (on 04.04.2019).

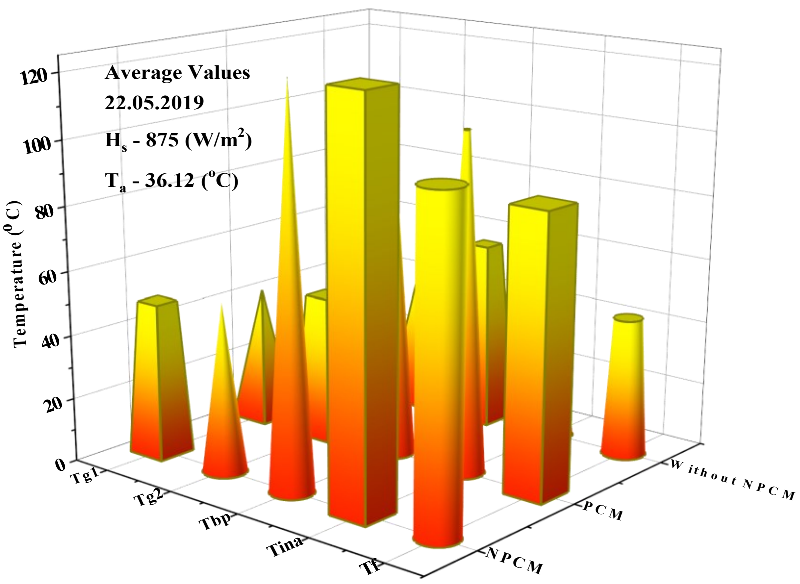

Figure 5(b). Average values of H_s, T_a, $T_{g1,2}$ T_{bp}, T_{ina} and T_f for SBCs (i) CSC (ii) with PCM (iii) with NPCM (on 22.05.2019).

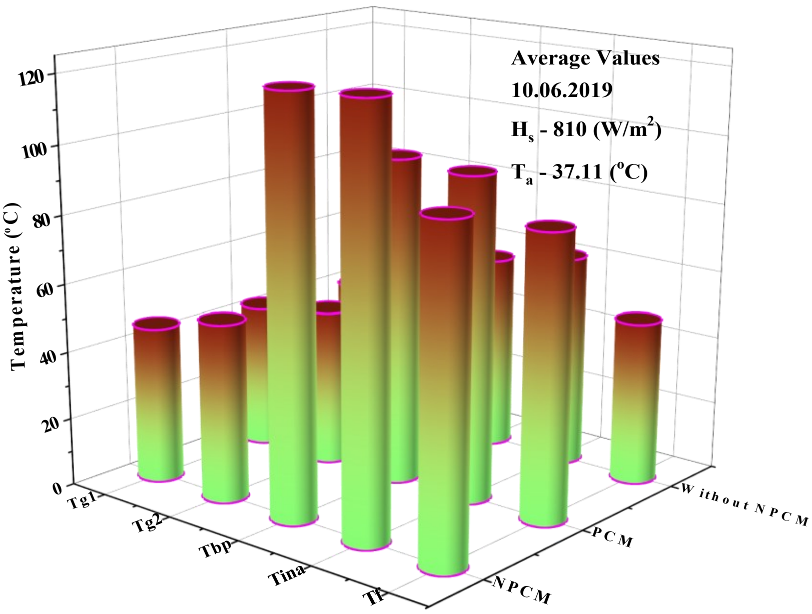

Figure 5(c). Average values of H_s, T_a, $T_{g1,2}$ T_{bp}, T_{ina} and T_f for SBCs (i) CSC (ii) with PCM (iii) with NPCM (10.06.2019).

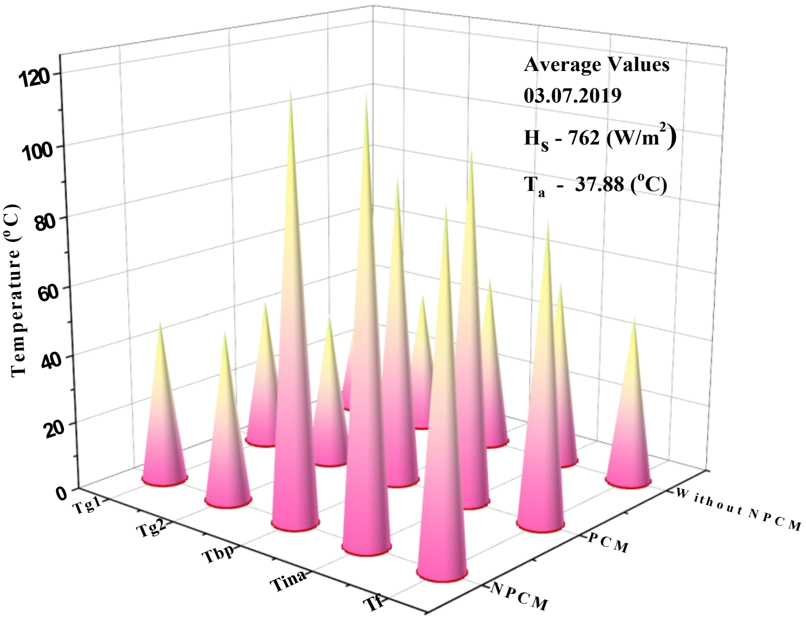

Figure 5(d). Average values of H_s, T_a, $T_{g1,2}$ T_{bp}, T_{ina} and T_f for SBCs (i) CSC (ii) with PCM (iii) with NPCM (03.07.2019).

The natural convection inside the cooker transfers the heat from the absorber to the second glass cover due to the resistance properties, the double-glazing configuration hinders further heat loss. Since the porous structure of nanocomposite ($MgAl_2O_4/Ni/Fe_2O_3$)-PCM was used in this study, more reflection loss was experimentally compared with the SBC with PCM and CSC. As shown in Figs.5(a, b, c, d), the average glass cover-1 temperature ranges from 40.10 to 43.66 ºC, and the glass cover-2 is in the range of about 41.77 to 51.33 ºC, with the average temperature values of 42.62 and 47.44 ºC for the glass covers 1 and 2 of the cookers.

Figs.5(a, b, c, d) also indicate the experimental measured average temperature values of the absorber (T_{bp}). It can be seen that the temperature values of the absorber plate increase within the period from 10:00 am to noon. The bar plate temperature was still 163.74°C at 18:00, where the conventional cooker's plate absorber temperature (CSC) and the cooker with the PCM were 113.34 °C, 147 °C, respectively.

It is concluded that the cooker with NPCM can produce a significantly higher absorber plate temperature than the cooker with PCM and the CSC. As illustrated in Figs.5(a, b, c, d) the internal air temperature of the cooker follows similar trends of the absorber's temperature as 102.56 °C, 147.2 °C, and 164.12 °C for the CSC, SBC with PCM, and SBC with NPCM working at 02:00 pm respectively. The developed SBCs were tested with water as the working fluid in contact with the plate absorber. Since the experimental set-up was installed on the high elevation (20 cm), the water boiled at around 98 °C owing to low atmospheric pressure. As shown in Figs.5(a, b, c, d), the boiling was started shorter than the expected time at noon. The temperature was continuously increased despite the cooker with PCM and the CSC with a fast temperature decreasing rate. At 14:00 the water temperature reached 69.21 °C in the CSC, 83.54 °C in the cooker with the PCM and 138.61 °C in the SBC with NPCM and reduced cooking times.

3.2 Discussion of solar cookers

In Figs.5(a, b, c, d - Exp.) and Fig.5(e -The.), experimental and theoretical temperature values of glass covers-1,2 ($T_{g1,2}$) under different weather conditions are presented. Comparing theoretical and experimental results on different days, there are few differences between values in days with higher values of solar radiation. The natural convection in glass covers is due to the resistance properties and therefore, it is concluded that since the single glazing (glass 1) temperature is relatively high, there is a significant convective heat loss from the top surface. Therefore, the double-glazing structure can be an efficient design to be used as the aperture surface in solar cookers.

Fig.5(e) indicates the measured and simulated values of the absorber's temperature (T_{bp}). On the other hand, the integration of double-glazing and PCM and NPCM coatings causes the plate absorber's temperature to be steadily increased due to the sensible thermal energy storage. Despite the decline in solar radiation, the obtained temperature of 163.74 °C at noon stayed constant during the remaining hours of days 04.04.2019, 22.05.2019, 10.06.2019, and 03.07.2019. The peak temperature achieved 163.74 °C, which was in good agreement for NPCM with the values reported in the preceding work [67] for similar ambient temperature and solar radiation values. The main goal of developing SBC with NPCM was introducing a highly efficient cooker with easy operation to help the society and the thermal energy storage in the bar plate absorber for incessant cooking by using the NPCM. The proposed cooking process is based on natural convection i.e., internal air temperature.

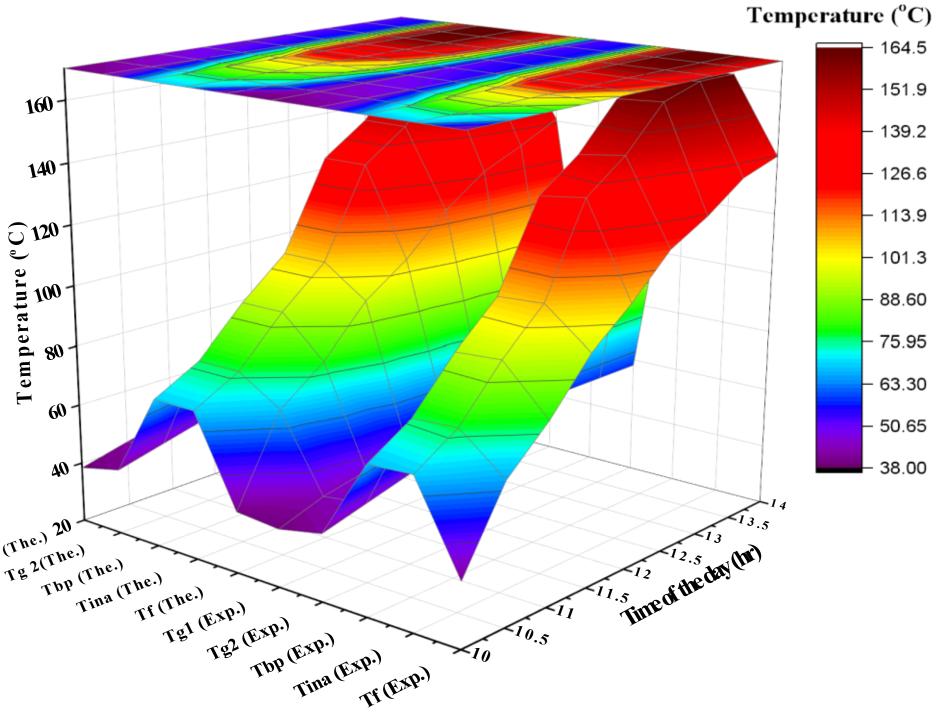

Figure 5(e). Experimental and theoretical temperature values of the glass cover 1, 2, bar plate, internal air, and food stuffiness for the SBC with NPCM and their variations with time of the day.

As illustrated in Figs.5(a, b, c, d), the cooker's internal air temperature has similar values with the absorber's temperature. However, it is lower than the expected values due to heat losses from the internal air to the ambient through the double-glazing glass cover. The internal air temperature of the developed cooker was growing steadily. Simultaneously, several declining points are observed in the internal temperature values recorded for the CSC due to the falling trend of solar radiation. The maximum internal air temperature for CSCs is reported around 127.96 °C by researchers. From other works, the internal air temperature of a typical CSC [63] and reflector-assisted SBC [68] working at 02:00 pm can be expected to be 102.56 °C for the CSC, 147.2 °C for the SBC with PCM, and 164.12 °C for the SBC with NPCM and Fig.5(e) shows a good agreement with these values for the system. As shown in this figure, there is a good agreement between the experimental results in Figs.5(a, b, c, d) and theoretical results in Fig.5(e). In Figs.6(a,b) compare the absorber plate's temperature in SBC with NPCM, with

PCM and CSC under different weather conditions (summer and winter). Additionally, the SBCs with a double-glass cover indicated a higher absorber's temperature. Consequently, the NPCM exhibits higher performance due to the shorter cooking time by [69] and increased temperature as shown in Fig.6(c). Moreover, the proposed cooker (with NPCM) has higher thermal conductivity than the CSC and the SBC with PCM. As shown in Fig.6(d), under the ambient temperature of 38.2°C, the vessel temperature was obtained as 165.5 $^{\circ}$C (SBC with NPCM), 147.2 $^{\circ}$C (SBC with PCM), and 112.34 °C (CSC), respectively, while the cooking rate was obtained as 90 min/3kg (SBC with NPCM), 140 min/3kg (SBC with PCM), and 180 min/3kg (CSC) as proved by [70].

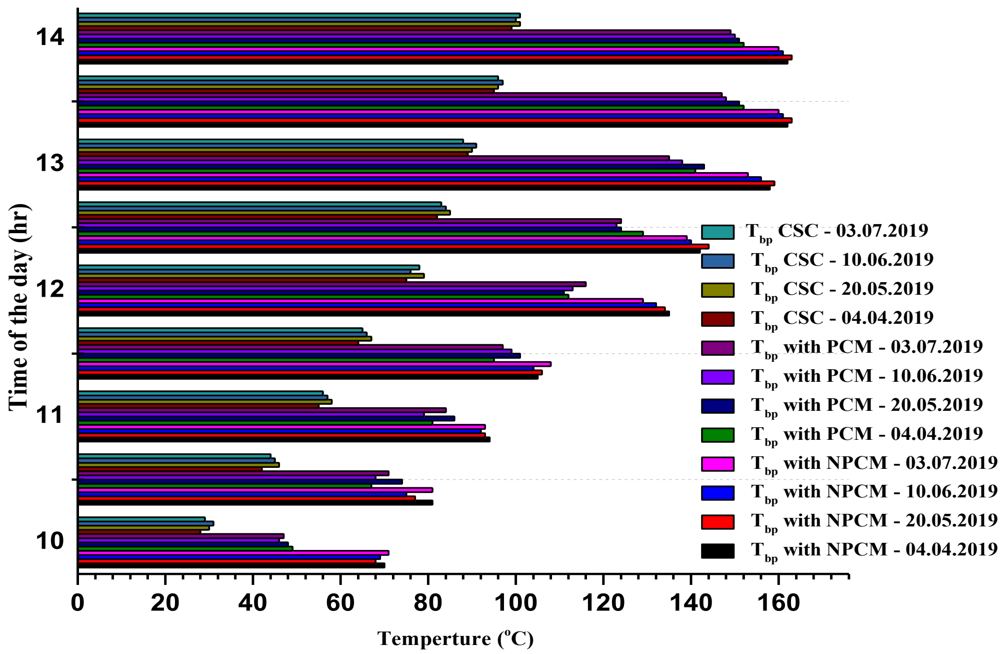

Figure 6(a). Variations of bar plate's temperatures under different weather conditions in various days of experiments for SBCs (i) CSC (ii) with PCM, and (iii) with NPCM.

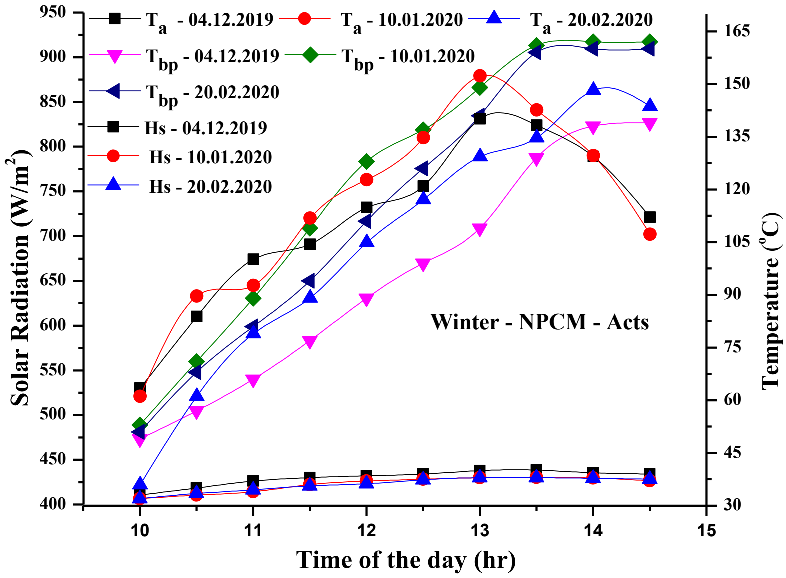

Figure 6(b). Variations H_s, T_a, $T_{g1,2}$ T_{bp}, T_{ina} and T_f of the SBC with NPCM with time of the day (in winter days).

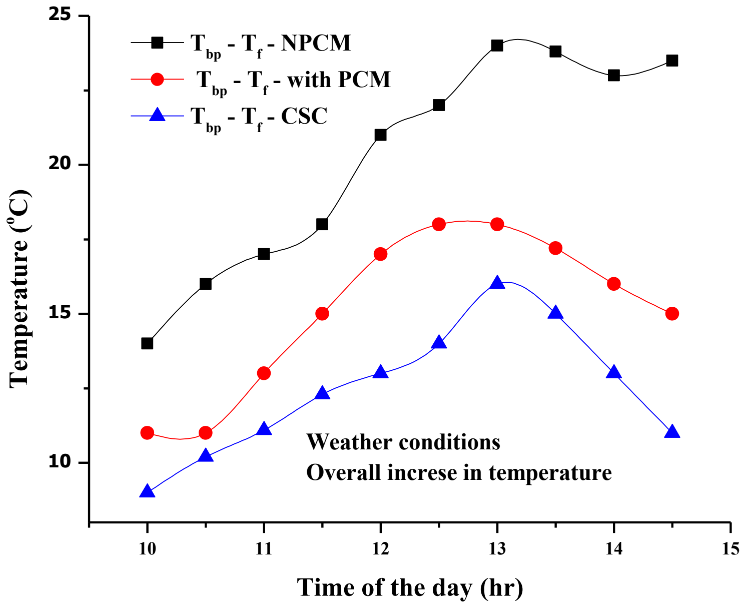

Figure 6(c). Overall temperature improvement of SBCs (i) with NPCM, (ii) with PCM (iii) CSC-Variations with the time of the day.

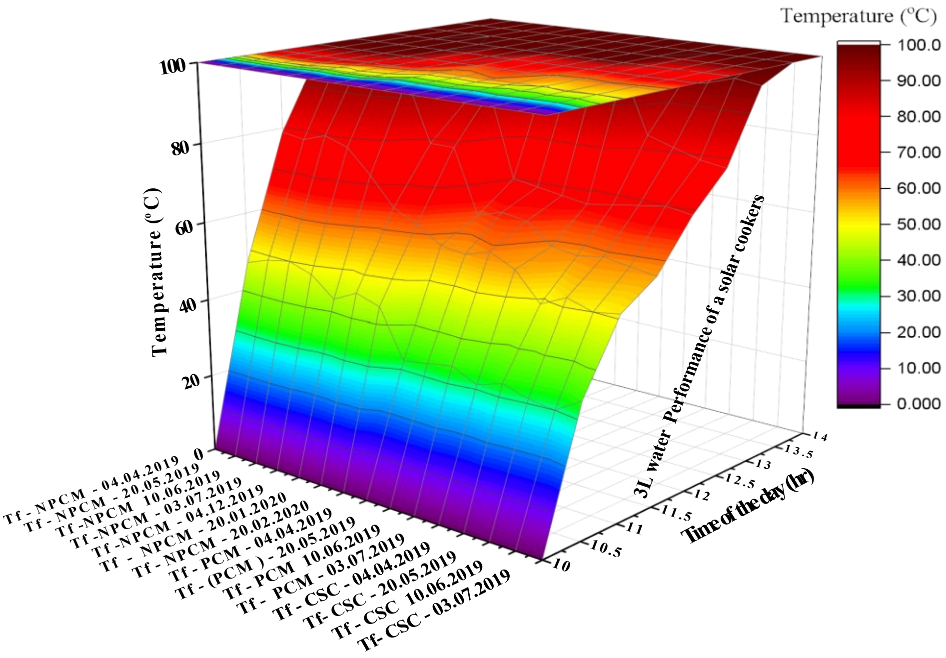

Figure 6(d). Water's (3L) temperature analysis of different solar cookers.

3.2.1 Cooking experiments using thermal image processing

A novel methodology was used to evaluate the thermal performance of SBCs with an enhanced plate absorber using thermal image processing. The rice boiling was studied as the cooking process with the segmentation technique. In this way, converting the boiled rice images to an appropriate version was conducted as one of the most crucial steps for segmentation purposes. Therefore, the rice boiling area was the input of thermal images, as depicted in Fig.7(a). Then the food images were processed using Haugh transforms, Otsu threshold, and median filter. Initially, thermal images were processed in Haugh transforms and attached to the points connected in edge views. The Otsu methods were used by the golly conditions of the threshold mixture. The cooking process images become sharpen using non-linear filters as shown in Fig.7(b) and demonstrated by [71].

The main goal of thermal image processing was to generate a more robust edge indicator function that was developed for the edge detection purpose based on fuzzy logic rules, X, and Y-axis shaped of the cooking rice to gray images. The indicator function's value was proportional to the intensity value, as shown in Fig.7(c). The proposed cooker was evaluated under the real cooking conditions for rice and the thermal image processing technique was used which was verified with segmentation rules in fuzzy logic rules. Therefore, the image processing was carried out based on the rules with suitable input and output values of black and yellow edge detection in rice food images. The performance of the NPCM is shown in Table 5, where the boiled items are eggs, beans, rice, and yam potatoes.

Table 5. Cooking performance of the SBC with NPCM, with PCM, and CSC.

Food item Cooked	Quantity (g)	Mixture Water (g)	Cooking Time (min) NPCM, PCM		Cooking Time (min) CSC	Remarks
Eggs	10nos	600	30	41	51	Done
Beans	1000	500	58	78	110	Done
Rice	1000	550	45	65	90	Done
yam	1000	450	41	61	75	Done
potatoes	1000	650	41	64	75	Done

The time demanded by the cooker with NPCM was in a range of 30 to 58 min compared to 41 to 78 min for the SBC with PCM and 51 to 110 min for the CSC to cook the same quantity of materials as investigated by Mahavar et al. [22] and Mullick et al. [72]. The thermal efficiency values ranged from 31.77-56.21% for SBC with NPCM, 24.77-45.20% for SBC with PCM, and 24.90-33.90% for the CSC, respectively. In terms of efficiency laws (Cramer's rule and fuzzy logic), the performance of the SBC with NPCM was enhanced, as depicted in Fig.8(a), which has also been demonstrated by Bhavani and Shanmugan [63] and Venugopal et al. [68]. The experimental tests revealed that the average efficiency of the system is 45.63 ± 2.21% (CSC), 49.21 ± 2.34% (SBC with PCM), 50.74 ± 2.09% (SBC with NPCM) as summarized in Table 6. The improved thermal efficiency values of SBCs were about (i) 6.7% for CSC, (ii) 8.6% for the SBC with PCM (iii) and, 9.7% for the SBC with NPCM, respectively.

Finally, it was found that the overall thermal performance of the SBC with NPCM is enhanced by about 11% as shown in Fig.8(b).

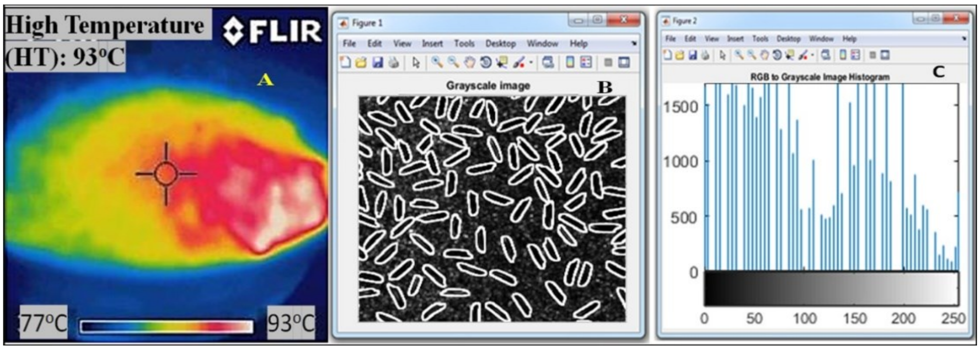

Figure 7. (a) Thermal image segmentation of solar cooking (rice); (A) Input thermal image of the cooking rice adapted from [73], (B) RGB2 gray scale image, (C) RGB2 gray scale image histogram.

Table 6. Analysis of the efficiency resulted from 1,000 g food stuffiness.

Efficiency Equations	Solar Cooker Absorption and Transmission	Cooker Side wall loss	Overall thermal Efficiency (%)	Modification
Y= 0.68 – 5.18x	0.68	5.18	45.63	CSC
Y = 0.67 – 5.10x	0.67	5.10	49.21	With PCM
Y = 0.72 – 5.18x	0.72	5.18	51.74	NPCM

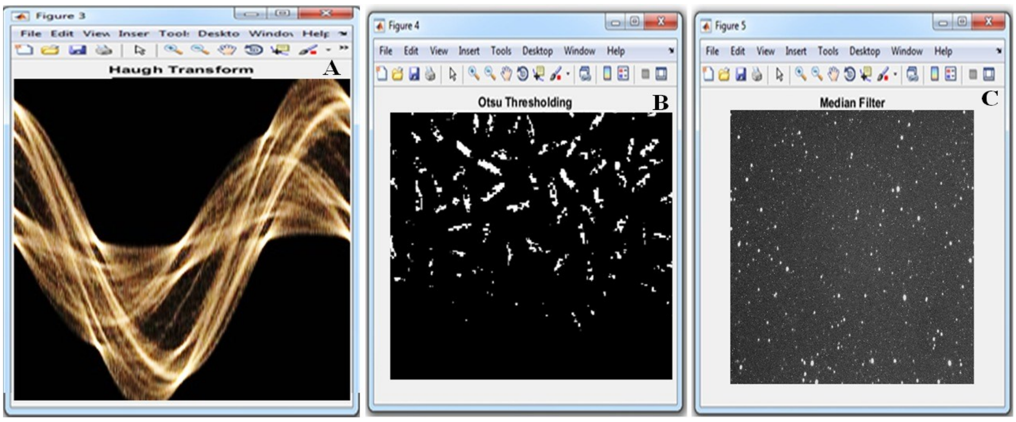

Figure 7. (b) Thermal images of rice; (A) Haugh transforms (B) Otsu thresholding (C) Median filter.

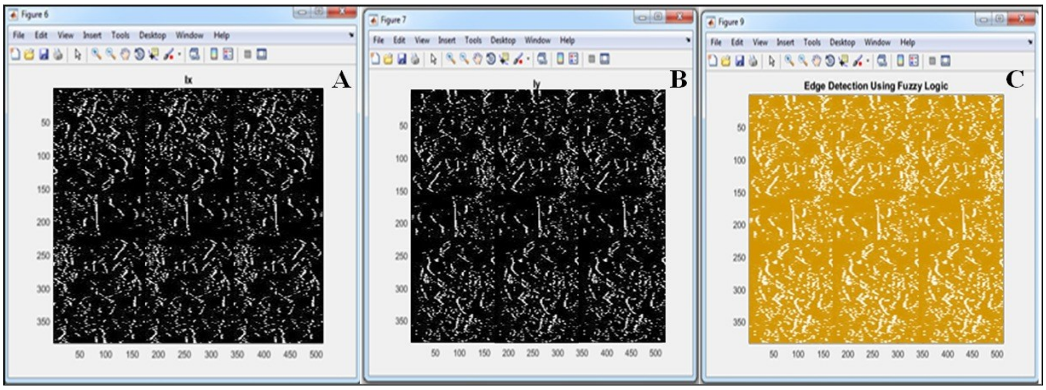

Figure 7. (c) Fuzzy logic analysis of thermal images of solar cooker; (a) X-axis, (b) Y-axis, (c) edge detection.

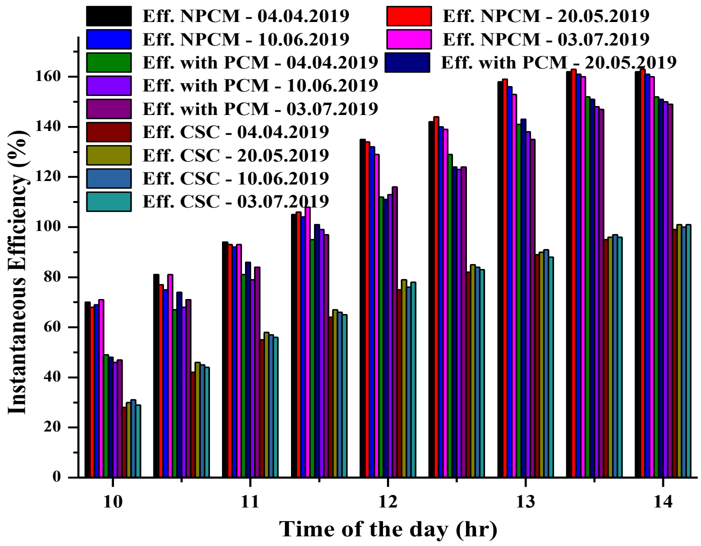

Figure 8. (a) Overall thermal efficiency of SBCs (i) with NPCM, (ii) with PCM (iii) CSC.

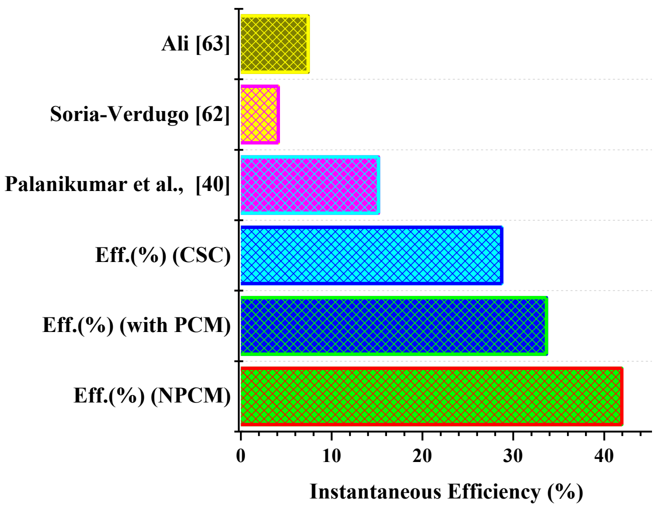

Figure 8(b). Comparison of overall improvement in SBCs (i) with NPCM, (ii) with PCM, and (iii) CSC.

3.1 Suggestions for future works

(i) Conducting the same testing procedure for other materials to expand the applicability of the proposed design.

(ii) Optimization should be applied to the proposed model to achieve higher performance values.

(iii) Long -term evaluation process should be carried out at different seasons.

4 Conclusion

In this study, three SBCs with PCM, with NPCM, and without NPCM were developed and their performance was experimentally and theoretically evaluated. The boiled rice food's thermal images were verified in both Cramer's and fuzzy rules. The sufficient internal heat transfer to the bottom sides, bar plate absorber, sidewalls, and the whole cooker were also investigated theoretically and experimentally. Further analysis may reveal the relationships between the characteristics in thermal images of the grain quality and digestibility. Finally, the main concluded points of the developed cooker are presented as:

- The thermal efficiency of the SBC was between 56.21 – 31.77% for the SBC with NPCM, 45.20 to 24.77% for the SBC with PCM, and 33.90 - 24.90% for the CSC.
- The performance of the SBC with NPCM was enhanced by adjusting the ambient temperature, fluid temperature, and wind speed.
- The results showed that the maximum absorber's temperature was 163.74 °C, 147 °C, and 113.34 °C for the SBC with NPCM, with PCM, and CSC, respectively.
- The SBC with NPCM provided the internal air temperature of 164.12 °C, and 147.2 °C and 102.56 °C for SBC with PCM and CSC, respectively.

- The SBC with NPCM required 30 to 58 min to cook different quantities of food materials, while the SBC with PCM and CSC needed 41 to 78 min and 51 to 110 min, respectively to do the same.

Notation of the novel cooker

a_m - Fraction melted

a_r - Fraction of the bar plate reacted

a_f - Fraction of the bar plate to absorbs

A-Inside heat air of the system (m^2)

b_{po}- Optical efficiency of bar plate temperature (ºC)

C_p- Specific heat of the cooker (kJ/kg K)

C_{bp} - Specific heat of the bar plate (kJ/kg K)

C_{av} - Average solar cooker temperature (ºC)

C_{bp} - Bar plate Specific heat (kJ/kg K)

C_{ap} - Average specific heat between Ti and T_f (kJ/kg K)

C_{lp} - Average specific heat between Tm and T_f (kJ/kg K)

C_{sp} - Average specific heat between Ti and Tm (kJ/kg K)

C_{pi}- Solar Cooking for power intervals (ºC)

C_{pw}- Specific heat of water (kJ/kg K)

C_a - Cooker area (vessel pots) (m^2)

c - Convective heat transfer coefficient (W/m^2)

dT - Total temperature of the system (ºC)

dt - Gain to energy for bar plate taken time derivative (S)

Gc - Glass cover one of the systems (ºC)

H_s - Solar irradiation (W/m^2)

m - Mass of the cooker (kg)

m_w- mass of water use cooking pot (kg)

m_{bp} - mass of bar plate (kg)

m_{bp} - Bar plate mass of heat storage medium (kg)

q_c - Convective heat transfer coefficient (W/m^2)

q_r - Radiative heat transfer coefficient (W/m^2)

$q_{c.sc-A}$ - Heat transfer convective rate of the cooker-to-cooker area (W/m^2)

$q_{R.sc-Gc1}$ - Heat transfer from reflective heat in the solar cooker to glass cover one (W/m^2)

$q_{c.a-Gc1}$ - Heat transfer from convective air to glass cover one (W/m^2)

$q_{r.sc-Gc1}$ - Heat transfer from reactive in the solar cooker to glass cover one (W/m^2)

$q_{R.bp-Gc1}$ - Heat transfer from reflective heat in bar plate to glass cover one (W/m^2)

$q_{R.Hs\,bp-Gc1}$ - Heat transfer from reflective solar irradiation in bar plate to glass cover one (W/m^2)

Q_{pcm-bp} - Total amount of PCM heat stored of the bar plate (kJ)

$Q_{F_}$PCM - Amount of thermal energy fraction use of PCM by the system (kJ)

Q - Total amount of heat stored of the bar plate (kJ)

Q_{f-bp} - Amount of thermal energy fraction use of bar plate by the system (kJ)

q - Heat transfer rate of the cooker (W/m^2)

$q_{r.Gc1-sc\,\_}$ heat transfer from radiative in glass cover one to solar cooker (ºC)

R - Reflector of the radiation temperature (W/m^2)

r - Radiative heat transfer coefficient (W/m^2)

Sc – Solar cooker (vessel) (kg)

T_g- Glass cover temperature (ºC)

T_a- Ambient temperature (ºC)

T_{sky} - Sky temperature (ºC)

T_{bp} - Bar plate temperature (ºC)

T_{swp} - Sidewall plate temperature of the system (ºC)

T_{fw} - Fluid water temperature (ºC)

T_{wi} - Initial water temperature (ºC)

T_m - Melting temperature (ºC)

T_f - Cooking final temperature (ºC)

T_i - Cooking initial temperature (ºC)

Δhm - Heat of fusion (kJ/kg)

Δh_r - Mixed PCM Endothermic heat of reaction of the solar box cooker (kJ/kg)

Δh_c - Heat of reaction of the cooker (kJ/kg)

ρ_g- Partial glass cover temperature (ºC)

α_{sc}- Absorptivity of the solar cooker in the system (ºC)

2θ - Reflected beam at an angle 2- theta from the incident beam by the sample - XRD.

Symbols

α_{bp} - Absorptivity of the bar plate

$\alpha_{g1,2}$ - Absorptivity of glass cover (1,2)

α_v - Absorptivity of the vessel

τ_{bp} - Transmissivity of the bar plate

τ_f - Transmissivity of the fluid

τ_v - Effective transmittance of the vessel

ρ_g - Density of the glass cover

ρ_{scf}- Density of the solar cooking materials fluid

References

[1] S. Gorjian, R. Singh, A. Shukla, A.R. Mazhar, On-farm applications of solar PV systems, in: S. Gorjian, A. Shukla (Eds.), Photovolt. Sol. Energy Convers., First, Elsevier, London, 2020: pp. 147–190. https://doi.org/10.1016/B978-0-12-819610-6.00006-5.

[2] S. Gorjian, H. Ebadi, F. Calise, A. Shukla, C. Ingrao, A review on recent advancements

in performance enhancement techniques for low-temperature solar collectors, Energy Convers. Manag. 222 (2020) 113246. https://doi.org/10.1016/j.enconman.2020.113246.

[3] S. Gorjian, B.N. Zadeh, L. Eltrop, R.R. Shamshiri, Y. Amanlou, Solar photovoltaic power generation in Iran: Development, policies, and barriers, Renew. Sustain. Energy Rev. 106 (2019) 110–123. https://doi.org/10.1016/j.rser.2019.02.025.

[4] R.E.N. Members, Renewables 2019 Global Status Report, 2019.

[5] P. Thamizharasu, S. Shanmugan, S. Gorjian, C.I. Pruncu, F.A. Essa, H. Panchal, M. Harish, Improvement of Thermal Performance of a Solar Box Type Cooker Using SiO2/TiO2 Nanolayer, Silicon. (2020). https://doi.org/10.1007/s12633-020-00835-1.

[6] S. Gorjian, B. Ghobadian, H. Ebadi, F. Ketabchi, S. Khanmohammadi, Applications of solar PV systems in desalination technologies, in: Photovolt. Sol. Energy Convers., Elsevier, 2020: pp. 237–274. https://doi.org/10.1016/B978-0-12-819610-6.00008-9.

[7] S. Gorjian, H. Sharon, H. Ebadi, K. Kant, F.B. Scavo, G.M. Tina, Recent technical advancements, economics and environmental impacts of floating photovoltaic solar energy conversion systems, J. Clean. Prod. 278 (2021) 124285. https://doi.org/10.1016/j.jclepro.2020.124285.

[8] S. Gorjian, B. Ghobadian, Solar desalination: A sustainable solution to water crisis in Iran, Renew. Sustain. Energy Rev. 48 (2015) 571–584. https://doi.org/10.1016/j.rser.2015.04.009.

[9] A. Saxena, Varun, S.P. Pandey, G. Srivastav, A thermodynamic review on solar box type cookers, Renew. Sustain. Energy Rev. 15 (2011) 3301–3318. https://doi.org/10.1016/j.rser.2011.04.017.

[10] H. Wang, J. Huang, M. Song, J. Yan, Effects of receiver parameters on the optical performance of a fixed-focus Fresnel lens solar concentrator/cavity receiver system in solar cooker, Appl. Energy. 237 (2019) 70–82.

https://doi.org/10.1016/j.apenergy.2018.12.092.

[11] A. Regattieri, F. Piana, M. Bortolini, M. Gamberi, E. Ferrari, Innovative portable solar cooker using the packaging waste of humanitarian supplies, Renew. Sustain. Energy Rev. 57 (2016) 319–326. https://doi.org/10.1016/j.rser.2015.12.199.

[12] S.Z. Farooqui, A review of vacuum tube based solar cookers with the experimental determination of energy and exergy efficiencies of a single vacuum tube based prototype, Renew. Sustain. Energy Rev. 31 (2014) 439–445. https://doi.org/10.1016/j.rser.2013.12.010.

[13] K. Schwarzer, M.E. V da Silva, Characterisation and design methods of solar cookers, Sol. Energy. 82 (2008) 157–163. https://doi.org/10.1016/j.solener.2006.06.021.

[14] S. Lokeswaran, M. Eswaramoorthy, Experimental studies on solar parabolic dish cooker with porous medium 1, Appl. Sol. Energy (English Transl. Geliotekhnika). 48 (2012) 169–174. https://doi.org/10.3103/S0003701X12030097.

[15] D. Chen, H. Wang, H. Qian, G. Zhang, S. Shen, Solar cooker effect test and temperature field simulation of radio telescope subreflector, Appl. Therm. Eng. 109 (2016) 147–154. https://doi.org/10.1016/j.applthermaleng.2016.08.048.

[16] M. González-Avilés, O.R. Urrieta, I. Ruiz, O.M. Cerutti, Design, manufacturing, thermal characterization of a solar cooker with compound parabolic concentrator and assessment of an integrated stove use monitoring mechanism, Energy Sustain. Dev. 45 (2018) 135–141. https://doi.org/10.1016/j.esd.2018.05.006.

[17] I. Edmonds, Low cost realisation of a high temperature solar cooker, Renew. Energy. 121 (2018) 94–101. https://doi.org/10.1016/j.renene.2018.01.010.

[18] Y. Zhao, H. Zheng, B. Sun, C. Li, Y. Wu, Development and performance studies of a novel portable solar cooker using a curved Fresnel lens concentrator, Sol. Energy. 174 (2018) 263–272. https://doi.org/10.1016/j.solener.2018.09.007.

[19] M. Singh, V.P. Sethi, On the design, modelling and analysis of multi-shelf inclined solar cooker-cum-dryer, Sol. Energy. 162 (2018) 620–636. https://doi.org/10.1016/j.solener.2018.01.045.

[20] M. Noman, A. Wasim, M. Ali, M. Jahanzaib, S. Hussain, H.M.K. Ali, H.M. Ali, An investigation of a solar cooker with parabolic trough concentrator, Case Stud. Therm. Eng. 14 (2019). https://doi.org/10.1016/j.csite.2019.100436.

[21] M. Hosseinzadeh, A. Faezian, S.M. Mirzababaee, H. Zamani, Parametric analysis and optimization of a portable evacuated tube solar cooker, Energy. 194 (2020) 116816. https://doi.org/10.1016/j.energy.2019.116816.

[22] S. Mahavar, P. Rajawat, R.C. Punia, N. Sengar, P. Dashora, Evaluating the optimum load range for box-type solar cookers, Renew. Energy. 74 (2015) 187–194. https://doi.org/10.1016/j.renene.2014.08.003.

[23] S.Z. Farooqui, An improved power free tracking system for box type solar cookers, Sol. Energy. 120 (2015) 100–103. https://doi.org/10.1016/j.solener.2015.07.021.

[24] S.B. Joshi, A.R. Jani, Photovoltaic and Thermal Hybridized Solar Cooker, ISRN Renew. Energy. 2013 (2013) 1–5. https://doi.org/10.1155/2013/746189.

[25] A. Harmim, M. Belhamel, M. Boukar, M. Amar, Experimental investigation of a box-type solar cooker with a finned absorber plate, Energy. 35 (2010) 3799–3802. https://doi.org/10.1016/j.energy.2010.05.032.

[26] S. Mahavar, N. Sengar, P. Dashora, Analytical model for electric back-up power estimation of solar box type cookers, Energy. 134 (2017) 871–881. https://doi.org/10.1016/j.energy.2017.06.060.

[27] A. Harmim, M. Merzouk, M. Boukar, M. Amar, Design and experimental testing of an innovative building-integrated box type solar cooker, Sol. Energy. 98 (2013) 422–433. https://doi.org/10.1016/j.solener.2013.09.019.

[28] Z. Guidara, M. Souissi, A. Morgenstern, A. Maalej, Thermal performance of a solar box cooker with outer reflectors: Numerical study and experimental investigation, Sol. Energy. 158 (2017) 347–359. https://doi.org/10.1016/j.solener.2017.09.054.

[29] A. Weldu, L. Zhao, S. Deng, N. Mulugeta, Y. Zhang, X. Nie, W. Xu, Performance evaluation on solar box cooker with reflector tracking at optimal angle under Bahir Dar climate, Sol. Energy. 180 (2019) 664–677. https://doi.org/10.1016/j.solener.2019.01.071.

[30] A. Saxena, N. Agarwal, Performance characteristics of a new hybrid solar cooker with air duct, Sol. Energy. 159 (2018) 628–637. https://doi.org/10.1016/j.solener.2017.11.043.

[31] A.A. Sagade, S.K. Samdarshi, P.J. Lahkar, N.A. Sagade, Experimental determination of the thermal performance of a solar box cooker with a modified cooking pot, Renew. Energy. (2019). https://doi.org/10.1016/j.renene.2019.11.114.

[32] G. Coccia, G. Di Nicola, S. Tomassetti, M. Pierantozzi, M. Chieruzzi, L. Torre, Experimental validation of a high-temperature solar box cooker with a solar-salt-based thermal storage unit, Sol. Energy. 170 (2018) 1016–1025. https://doi.org/10.1016/j.solener.2018.06.021.

[33] P.M. Cuce, Box type solar cookers with sensible thermal energy storage medium: A comparative experimental investigation and thermodynamic analysis, Sol. Energy. 166 (2018) 432–440. https://doi.org/10.1016/j.solener.2018.03.077.

[34] L. NKhonjera, M. Kuboth, A. König-Haagen, G. John, C. King'ondu, D. Brüggemann, T. Bello-Ochende, Experimental Investigation of a Finned Pentaerythritol-based Heat Storage Unit for Solar Cooking at 150-200℃, Energy Procedia. 93 (2016) 160–167. https://doi.org/10.1016/j.egypro.2016.07.165.

[35] G. John, A. König-Haagen, C.K. King'ondu, D. Brüggemann, L. Nkhonjera, Galactitol

as phase change material for latent heat storage of solar cookers: Investigating thermal behavior in bulk cycling, Sol. Energy. 119 (2015) 415–421. https://doi.org/10.1016/j.solener.2015.07.003.

[36] A. Lecuona, J.I. Nogueira, R. Ventas, M. del C. Rodríguez-Hidalgo, M. Legrand, Solar cooker of the portable parabolic type incorporating heat storage based on PCM, Appl. Energy. 111 (2013) 1136–1146. https://doi.org/10.1016/j.apenergy.2013.01.083.

[37] A.G. Bhave, K.A. Thakare, Development of a solar thermal storage cum cooking device using salt hydrate, Sol. Energy. 171 (2018) 784–789. https://doi.org/10.1016/j.solener.2018.07.018.

[38] C.R. Chen, A. Sharma, S.K. Tyagi, D. Buddhi, Numerical heat transfer studies of PCMs used in a box-type solar cooker, Renew. Energy. 33 (2008) 1121–1129. https://doi.org/10.1016/j.renene.2007.06.014.

[39] A.G. Bhave, C.K. Kale, Development of a thermal storage type solar cooker for high temperature cooking using solar salt, Sol. Energy Mater. Sol. Cells. 208 (2020). https://doi.org/10.1016/j.solmat.2020.110394.

[40] S. Geddam, G.K. Dinesh, T. Sivasankar, Determination of thermal performance of a box type solar cooker, Sol. Energy. 113 (2015) 324–331. https://doi.org/10.1016/j.solener.2015.01.014.

[41] E. Cuce, Improving thermal power of a cylindrical solar cooker via novel micro/nano porous absorbers: A thermodynamic analysis with experimental validation, Sol. Energy. 176 (2018) 211–219. https://doi.org/10.1016/j.solener.2018.10.040.

[42] S.S. Ghosh, P.K. Biswas, S. Neogi, Thermal performance of solar cooker with special cover glass of low-e antimony doped indium oxide (IAO) coating, Appl. Therm. Eng. 113 (2017) 103–111. https://doi.org/10.1016/j.applthermaleng.2016.10.185.

[43] G.G. Jang, J.W. Klett, J. McFarlane, A. Ievlev, K. Xiao, J.K. Keum, M. Yoon, P. Im,

M.Z. Hu, J.E. Parks, Efficient Solar-Thermal Distillation Desalination Device by Light Absorptive Carbon Composite Porous Foam, Glob. Challenges. (2019) 1900003. https://doi.org/10.1002/gch2.201900003.

[44] E. AlShamaileh, Testing of a new solar coating for solar water heating applications, Sol. Energy. 84 (2010) 1637–1643. https://doi.org/10.1016/j.solener.2010.06.003.

[45] S. Shanmugan, S. Palani, B. Janarthanan, Productivity enhancement of solar still by PCM and Nanoparticles miscellaneous basin absorbing materials, Desalination. (2018) 186–198. https://doi.org/10.1016/j.desal.2017.11.045.

[46] S. Bhavani, S. Shanmugan, P. Selvaraju, C. Monisha, V. Suganya, Fuzzy interference treatment applied to energy control with effect of box type affordable solar cooker, in: Mater. Today Proc., Elsevier Ltd, 2019: pp. 1280–1290. https://doi.org/10.1016/j.matpr.2019.06.590.

[47] G. Palanikumar, S. Shanmugan, C. Vengatesan, S. Periyasam, Evaluation of fuzzy inference in box type solar cooking food image of thermal effect, Environ. Sustain. Indic. (2019) 100002. https://doi.org/10.1016/j.indic.2019.100002.

[48] A.A. El-Sebaii, A. Ibrahim, Experimental testing of a box-type solar cooker using the standard procedure of cooking power, Renew. Energy. 30 (2005) 1861–1871. https://doi.org/10.1016/j.renene.2005.01.007.

[49] N.M. Nahar, Performance and testing of a hot box storage solar cooker, Energy Convers. Manag. 44 (2003) 1323–1331. https://doi.org/10.1016/S0196-8904(02)00113-9.

[50] A.H. Algifri, H.A. Al-Towaie, Efficient orientation impacts of box-type solar cooker on the cooker performance, Sol. Energy. 70 (2001) 165–170. https://doi.org/10.1016/S0038-092X(00)00136-5.

[51] S. Kumar, Thermal performance study of box type solar cooker from heating characteristic curves, Energy Convers. Manag. 45 (2004) 127–139.

https://doi.org/10.1016/S0196-8904(03)00103-1.

[52] A.E. Kabeel, M. Abdelgaied, Improving the performance of solar still by using PCM as a thermal storage medium under Egyptian conditions, Desalination. 383 (2016) 22–28. https://doi.org/10.1016/j.desal.2016.01.006.

[53] G. Oturanç, N. Özbalta, A. Güngör, Performance analysis of a solar cooker in Turkey, Int. J. Energy Res. 26 (2002) 105–111. https://doi.org/10.1002/er.769.

[54] D. Buddhi, S.D. Sharma, A. Sharma, Thermal performance evaluation of a latent heat storage unit for late evening cooking in a solar cooker having three reflectors, Energy Convers. Manag. 44 (2003) 809–817. https://doi.org/10.1016/S0196-8904(02)00106-1.

[55] X. Jin, X. Zhang, Thermal analysis of a double layer phase change material floor, Appl. Therm. Eng. 31 (2011) 1576–1581. https://doi.org/10.1016/j.applthermaleng.2011.01.023.

[56] Y. Cong, Z. Li, Y. Zhang, Q. Wang, Q. Xu, Synthesis of α-Fe 2O 3/TiO 2 nanotube arrays for photoelectro-Fenton degradation of phenol, Chem. Eng. J. 191 (2012) 356–363. https://doi.org/10.1016/j.cej.2012.03.031.

[57] Q. Wang, N. Zhu, E. Liu, C. Zhang, J.C. Crittenden, Y. Zhang, Y. Cong, Fabrication of visible-light active Fe 2 O 3 -GQDs/NF-TiO 2 composite film with highly enhanced photoelectrocatalytic performance, Appl. Catal. B Environ. 205 (2017) 347–356. https://doi.org/10.1016/j.apcatb.2016.11.046.

[58] Y. Cong, Y. Ge, T. Zhang, Q. Wang, M. Shao, Y. Zhang, Fabrication of Z-Scheme Fe2O3 –MoS2 –Cu2O Ternary Nanofilm with Significantly Enhanced Photoelectrocatalytic Performance, Ind. Eng. Chem. Res. 57 (2018) 881–890. https://doi.org/10.1021/acs.iecr.7b04089.

[59] J. Zhang, L. Huang, Z. Lu, Z. Jin, X. Wang, G. Xu, E. Zhang, H. Wang, Z. Kong, J. Xi, Z. Ji, Crystal face regulating MoS2/TiO2(001) heterostructure for high photocatalytic

activity, J. Alloys Compd. 688 (2016) 840–848. https://doi.org/10.1016/j.jallcom.2016.07.263.

[60] R. Mamlook, O. Badran, Fuzzy sets implementation for the evaluation of factors affecting solar still production, Desalination. 203 (2007) 394–402. https://doi.org/10.1016/j.desal.2006.02.024.

[61] A. Duarte, L. Carrão, M. Espanha, T. Viana, D. Freitas, P. Bártolo, P. Faria, H.A. Almeida, Segmentation Algorithms for Thermal Images, Procedia Technol. 16 (2014) 1560–1569. https://doi.org/10.1016/j.protcy.2014.10.178.

[62] N. Senthilkumaran, R. Rajesh, Edge Detection Techniques for Image Segmentation – A Survey of Soft Computing Approaches, Int. J. Recent Trends Eng. 1 (2009) 250–254.

[63] B. S, S. S, S. P, High Performance of Solar Cooker by Heat Transfer Mode Condition System Using Fuzzy Logic Controller Applications, Int. J. Eng. Technol. 7 (2018) 278. https://doi.org/10.14419/ijet.v7i4.10.20912.

[64] P.A. Funk, Evaluating the international standard procedure for testing solar cookers and reporting performance, Sol. Energy. 68 (2000) 1–7. https://doi.org/10.1016/S0038-092X(99)00059-6.

[65] A. Harmim, M. Boukar, M. Amar, Experimental study of a double exposure solar cooker with finned cooking vessel, Sol. Energy. 82 (2008) 287–289. https://doi.org/10.1016/j.solener.2007.10.008.

[66] M. Hussain, K.C. Das, A. Huda, The performance of a box-type solar cooker with auxiliary heating, Renew. Energy. 12 (1997) 151–155. https://doi.org/10.1016/S0960-1481(97)00037-2.

[67] F. Yettou, B. Azoui, A. Malek, N.. Panwar, A. Gama, T. Arrif, H. Merarda, Comparative assessment of two different designs of box solar cookers under algerian sahara conditions, Rev. Des Energies Renouvelables. 18 (2015) 227 – 234.

[68] D. Venugopal, J. Chandrasekaran, B. Janarthanan, S. Shanmugan, S. Kumar, Parametric optimization of a box-type solar cooker with an inbuilt paraboloid reflector using Cramer's rule, Int. J. Sustain. Energy. 31 (2012) 213–227. https://doi.org/10.1080/1478646X.2011.558197.

[69] A. Soria-Verdugo, Experimental analysis and simulation of the performance of a box-type solar cooker, Energy Sustain. Dev. 29 (2015) 65–71. https://doi.org/10.1016/j.esd.2015.09.006.

[70] B.S.M. Ali, Design and testing of Sudanese solar box cooker, Renew. Energy. 21 (2000) 573–581. https://doi.org/10.1016/S0960-1481(00)00089-6.

[71] N. Otsu, THRESHOLD SELECTION METHOD FROM GRAY-LEVEL HISTOGRAMS., IEEE Trans Syst Man Cybern. SMC-9 (1979) 62–66. https://doi.org/10.1109/tsmc.1979.4310076.

[72] S.C. Mullick, T.C. Kandpal, A.K. Saxena, Thermal test procedure for box-type solar cookers, Sol. Energy. 39 (1987) 353–360. https://doi.org/10.1016/S0038-092X(87)80021-X.

[73] G. Palanikumar, S. Shanmugan, V. Chithambaram, Solar cooking thermal image processing applied to time series analysis of fuzzy stage and inconsiderable Fourier transform method, Materials Today: Proceedings 34 (2021) 460–468